An OP-FTIR Trace Gas Observatory: Design, Automation, and Applications

By
Keane Tobin

A Thesis Submitted to
Saint Mary's University, Halifax, Nova Scotia
in Partial Fulfilment of the Requirements for
the Degree of Master of Science in Applied Science

May 2018, Halifax, Nova Scotia

Approved By:	Dr. Aldona Wiacek Supervisor
Approved By:	Dr. Roby Austin Committee Member
Approved By:	Dr. Jason Clyburne Committee Member
Approved By:	Dr. David Risk External Examiner
Date:	May 1 2018

Abstract

An OP-FTIR Trace Gas Observatory: Design, Automation, and Applications

By Keane Tobin

Atmospheric trace gas measurements aid in the understanding of air quality, climate change, and biogeochemical processes. Open-Path Fourier Transform Infrared (OP-FTIR) spectroscopy can be used to measure many infrared active trace gases in a lower tropospheric path. The atmospheric observatory designed as part of this project will enable long-term OP-FTIR trace gas datasets to be collected and examined by the Tropospheric Remote Sensing Laboratory (TRSL) and external users.

An application of utilizing OP-FTIR data is explored in studying the detectability of biomass burning emissions from near- and far-range wildfire sources in Halifax. Atmospheric transport modeling and infrared spectrum retrievals are used to determine that transported emission detectability is likely given proper environmental conditions and sufficiently optimized retrievals. The study involved start-to-finish data analysis, from spectrum acquisition, through spectral analysis and retrieval optimization, to time series analysis of trace gas concentrations.

May 1 2018

Acknowledgements

This project would not have been possible without the efforts of many individuals. I would first like to thank Dr. Aldona Wiacek for guiding me though every aspect of this work. Also, thanks to Dr. Roby Austin and Dr. Jason Clyburn for the advice and direction. Thank you to Dr. David Risk for the examination of my work and his excellent input.

Thanks to Dr. Li Li, Morgan Mitchell, and Taylor Gray for creating the tools and helping to collect the data that made this project possible.

I would also like to acknowledge Peter Maas from Bruker Inc. for the quick and informative responses regarding the spectrometer and Dr. David Griffith for the support with running MALT for retrievals. Also thank you to Facilities Management at Saint Mary's University for working hard to find a home for the spectrometer.

For financial support, thank you to Saint Mary's University and NSERC and CFI for funding this project and enabling this research in the Maritimes.

Finally thank you to my parents who gave me the foundation that enabled me to complete this project. Also, to Mia for all the support and for continuously encouraging me.

Table of Contents

1. Introduction 1
1.1. Atmospheric Trace Gases 1
1.2. Fourier Transform Infrared Spectroscopy (FTIR) 4
1.3. Open Path Fourier Transform Infrared Spectroscopy (OP-FTIR) 9
1.4. OP-FTIR Applications 10
1.5. Bruker Spectrometer Design and Performance 11
1.6. Scope of Work 14
2. Observatory Design and Automation 15
2.1. Detection Limits and Path Length 15
2.2. Spectrometer Enclosure 19
2.3. Retroreflector Enclosure 26
2.4. Automation 29
2.5. Path Bending Flat Mirror 33
3. Biomass Burning Case Study 36
3.1. Biomass Burning Tracer Gases 37
3.2. Transport Modeling of Biomass Burning Emissions 38
3.3. Retrieval Method 43
3.4. Conclusions on Detectability 68
4. Future Work 69
Appendix A: OP-FTIR Standard Operating Procedure 71
Appendix B: HYSPLIT Trajectories 83
Appendix C: Observatory RFP 84
Appendix D: Retroreflector Door Force Requirements 88
Appendix E: Observatory Automation Solution Parts List 89
Appendix F: Weather Control Python Script 90
5. References 94

List of Figures

Figure 1: Map of the NDACC IRWG Stations (https://www2.acom.ucar.edu/irwg/sites). 4
Figure 2: The stretching and bending of CO_2 (Adapted from: Banwell & MacCash, 1994). 6
Figure 3: Vibration-Rotation spectra of CO_2 centered at 2350 cm^{-1} for 1 ppm in a 1 meter path at 296 K (PNNL database). 7
Figure 4: Schematic of a generic OP-FTIR internal and external operation (Adapted from: Jarvis, 2003). 9
Figure 5: Open Path System by Bruker annotated with a typical recorded spectrum (Adapted from: Bruker, 2013). 11
Figure 6: Internal optics of the Bruker OP-FTIR showing A) infrared source, B) aperture wheel, C) beam splitter, and D) detector (Peter Maas, personal communication, November 2017). 13
Figure 7: Two-way path length versus peak signal in received spectra with best fit. 18
Figure 8: Bruker supplied intensity versus two-way path length (Adapted from: Bruker, 2015). 18
Figure 9: Observatory Location on the Student Center Building at SMU, adapted from Google Maps, 2017. 20
Figure 10: Viewshed from observatory, indicating suitable retro locations (Courtesy: Greg Baker, SMU). 21
Figure 11: Proposed observatory schematic. 23
Figure 12: Rendering of observatory (wind mast not to scale). 23
Figure 13: Window vertical placement model, showing minimum 65” window center from floor. 24
Figure 14: Student Center Building rooftop modification plans (Barry McNeil, personal communication, March 2018). 25
Figure 15: Retroreflector housing fitted with actuators in closed (left) and open (right) position. Red arrows indicate linear actuators. 27
Figure 16: Retroreflector housing receiver-side door control electrical schematic. 29
Figure 17: The USB to GPIO board wired to the RF transmitter. 31
Figure 18: An electrical diagram of the laptop to RF transmitter interface on the transmitter side. 31
Figure 19: GUI of retroreflector control program with weather status (Good/Bad), retro door status (Open/Closed), and action buttons on the right to override the algorithm’s decision. 33
Figure 20: Path extending flat mirror configurations. 34
Figure 21: Flat mirror, mount, tripod head, and tripod. 35
Figure 22: Orientation of OP-FTIR during biomass burning event measurements. 38
Figure 23: Fire counts and estimated emission area in 2016 biomass burning case study. 39

Figure 24: Sample HYSPLIT trajectory maps for air masses from the Fort McMurray and Seven Mile Lake events. Yellow squares represent the boxes around Halifax used to identify if transport occurs or not. 41
Figure 25: NAAMES vertical aerosol profile on May 13th where the star marks the location of Halifax (Denise Lineberry, 2016). 43
Figure 26: Example fit for CO_2. 45
Figure 27: Schematic of MATLAB scripts to process large data sets of OP-FTIR observations. Each box represents a MATLAB script. 49
Figure 28: Example fit from August 9, 2016 at 12:25 of each retrieved biomass burning tracer identified in Table 3. 51
Figure 29: Housekeeping file for CH_3COOH retrieval 55
Figure 30: RMS of the residual (0.1 = 10%) versus infrared signal for target trace gases for a series of individual retrievals shown in Figure 32. 56
Figure 31: Plot of shipping locations and routes during peak of CO event on August 10 from 09:00 – 10:00. 57
Figure 32: Full time series of retrieval results from Seven Mile Lake wildfire campaign in 2016. 62
Figure 33: Environmental parameters during Seven Mile Lake wildfire event in 2016. .. 63
Figure 34: Relationships of trace gases to CO (emission factor decrease for each gas from top to bottom). 65
Figure 35: CH_3COOH versus CO during transport time during Seven Mile Lake biomass burning event (August 8 - 15). 66

List of Tables

Table 1: A selection of trace gases with detection limits and absorption simulation results at typical one-way paths. Path for percent absorption scales linearly (e.g. for 1% absorption the path will double). 17
Table 2: Biomass burning event locations, sizes, and temporal burn ranges (in 2016). .. 36
Table 3: Trace gases used as tracers of biomass burning. 37
Table 4: Nova Scotia wildfire "likely transport" arrival times based on 24 hour trajectory calculations initiated every 3 hours for the wildfire duration. Full detailed table in Appendix B: HYSPLIT Trajectories. 42
Table 5: Spectral fitting parameters within MALT software (Griffith, 2012)..... 47
Table 6: Correlation of biomass burning tracer gases with CO on August 10th from 13:00 – 15:00 (time of predicted plume transport to Halifax). 66
Table 7: Correlation of biomass burning tracer gases with CO on August 10th from 08:00 – 11:00 (time of observed elevated CO in Halifax). 67

Glossary of Terms

- AB – Alberta
- C_2H_6 – Ethane
- CH_3COOH – Acetic Acid
- CH_3OH – Methanol
- CH_4 – Methane
- CO – Carbon Monoxide
- CO_2 – Carbon Dioxide
- FTIR – Fourier Transform Infrared (Spectrometer)
- GDAS – Global Data Assimilation System
- GPIO – General Purpose Input Output
- GUI – Graphical User Interface
- H_2CO – Formaldehyde
- H_2O – Water
- HCN – Hydrogen Cyanide
- HYSPLIT – Hybrid Single Particle Lagrangian Integrated Trajectory Model
- MALT – Multiple Atmospheric Layer Transmittance (Retrieval Algorithm)
- MCT – Mercury Cadmium Telluride (Detector)
- N_2 – Nitrogen
- N_2O – Nitrous Oxide
- NAAMES – North Atlantic Aerosols and Marine Ecosystems Study
- NAM – North America Mesoscale Forecast System
- NAPS – National Air Pollution Surveillance
- NDACC – Network for the Detection of Atmospheric Composition Change
- NH_3 – Ammonia
- NLLS – Non-Linear Least Squares
- NO_X – Nitrogen Oxides
- NS – Nova Scotia
- NSE – Nova Scotia Environment
- O_2 – Oxygen
- O_3 – Ozone
- OPD – Optical Path Difference
- OP-FTIR – Open-Path Fourier Transform Infrared (Spectrometer)
- PM2.5 – Particle Matter < 2.5µm Diameter
- RF – Radio Frequency
- RFP – Request for Proposals
- RMS – Root Mean Squared
- SMU – Saint Mary's University
- SO_2 – Sulphur Dioxide
- TCCON – Total Carbon Column Observing Network
- TRSL – Tropospheric Remote Sensing Laboratory
- VOC – Volatile Organic Compounds

1. Introduction

1.1. Atmospheric Trace Gases

The atmosphere creates a habitable environment for humans and all other species living on Earth. It keeps the planet warmer than 0 °C in a global annual mean sense through the greenhouse effect and promotes the hydrological cycle that supports life on all continents. The composition of the atmosphere primality consists of nitrogen (N_2), oxygen (O_2), and various trace gases that are impacted by anthropogenic and biogenic emissions from primary sources as well as species produced via secondary chemical reactions, e.g. the secondary production of ground-level ozone (O_3) from primary emitted precursors like nitrogen oxides (NO_X), carbon monoxide (CO), and volatile organic compounds (VOCs) (Jacob, 1999).

The large increase of carbon dioxide (CO_2) in the atmosphere over the past two centuries has been attributed to anthropogenic sources. Changes in concentrations of CO_2 and other greenhouse gases influence the radiation budget of the atmosphere through increased absorption of upwelling thermal radiation and have resulted in increased amounts of solar energy being trapped as heat as a result of the greenhouse effect. The increased heat absorption resulted in a warming between 0.5 to 1.3 ^{o}C from 1880 to 2012 (*IPCC AR5,* 2013). This temperature increase includes the effects of methane (CH_4), which is a potent greenhouse gas, emitted largely from anthropogenic sources such as agriculture and fossil fuel production (twice the volume of natural sources) and also

nitrous oxide (N_2O), another potent greenhouse gas which has an equal natural and antropogenic sources (largely from agriculture) (Jacob, 1999).

In general, gases other than O_2 and N_2, that exist in smaller quantities (<1%) are referred to as trace gases and can have large impacts on atmospheric chemistry and the climate. Knowledge of trace gas concentration levels is fundamental to the characterization of air quality, which is influenced by local industry, long-range pollution transport, and biogenic emissions, both direct and in the form of precursor gases. Poor ground-level air quality has environmental and human health implications, e.g. plant tissue oxidation caused by O_3 and respiratory difficulties. Oxides of nitrogen (NO_X = NO + NO_2) and sulphur dioxide (SO_2) are also emitted from fossil fuel burning and are toxic to humans in higher concentrations as well as leading to sulfate and nitrate particle formation. Finally, VOCs are another large family of organic compounds with low boiling points (e.g. aldehydes and ketones) that readily react in the atmosphere resulting in a wide range of chemical products, including O_3 and secondary organic aerosols, which are major components of photochemical smog (Shepardson, 2012).

Given the impacts that trace gases can have on environmental and human health, monitoring their concentrations over time is necessary and increases our understanding of air quality and climate change. There are a variety of methods to monitor gases in the atmosphere either *in situ* with gas sensors operating on many chemical or physical detection principles, or by remote sensing using spectroscopic techniques.

Current air quality monitoring in Nova Scotia (NS) is primarily performed by Environment and Climate Change Canada and Nova Scotia Environment (NSE). Data collected by these organizations become part of the National Air Pollution Surveillance (NAPS) Network. The closest NAPS site in proximity (<2 km) to the Saint Mary's University (SMU) campus is located at 1645 Barrington Street in Halifax, NS. This site measures CO, NO_X, O_3, SO_2, and particulate matter under 2.5 μm diameter (PM2.5), which are all regulated compounds. Additionally, the NSE station analyzes 24-hour canister samples, collected every sixth day, for more than 167 VOCs (Nova Scotia Environment, 2016).

Other sources of atmospheric composition data in Nova Scotia come from very sparse field campaigns (Millet et al., 2006) and several satellite missions. Satellite-based instruments measure CO, CO_2, CH_4, NO, NO_2, O_3, SO_2, and others (World Meteorological Organization, 2018). Satellite-based observations are excellent at identifying large-scale spatial and temporal trends in the atmosphere but have limitations when it comes to local ground-level air quality because of their often reduced sensitivity to surface air.

These satellite observations are often validated by networks of solar absorption Fourier transform infrared (FTIR) spectrometers such as the Total Column Carbon Observing Network (TCCON) and the Network for the Detection of Atmospheric Composition Change (NDACC). The measurements in these networks consist of total column measurements, with limited vertical profiling, similar to the satellite-based measurements. There are 29 TCCON stations and 25 NDACC stations, shown in Figure 1, but none located near the Atlantic coast of Canada, the closest being the Toronto site approximately 1300 km away.

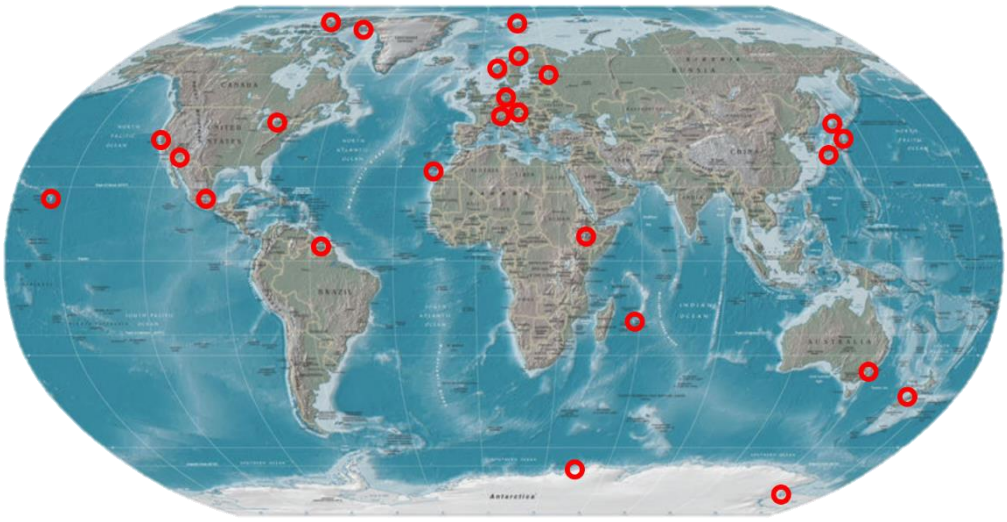

Figure 1: Map of the NDACC IRWG Stations (https://www2.acom.ucar.edu/irwg/sites).

The current networks of *in situ*, ground based total column, aircraft, balloon, and satellite measurements have given scientists solid databases of observations to study the atmosphere, however there is a need for tropospheric atmospheric composition measurements to broaden information on local sources and impacts of a changing climate on the air we breathe for the purpose of global and regional atmospheric chemistry model testing. The atmospheric observatory that is the subject of this MSc project will help fill this measurement gap.

1.2. Fourier Transform Infrared Spectroscopy (FTIR)

Spectroscopy is the study of the interaction of electromagnetic radiation and matter (Banwell & MacCash, 1994). Electromagnetic radiation can be described as massless photon particles or self-propagating electric and magnetic fields, which exhibit wave properties, including wavelength (λ), frequency (ν), spatial frequency or wavenumber ($\bar{\nu} = \lambda^{-1}$), and an energy ($E = h\nu$, where h is Plank's constant). As these waves propagate

through a medium, they can interact with the molecules present. Each molecule has an energy composed of electronic energy of valence shell electron position, rotational energy due to rotation about its center of mass, and vibrational energy of the displacements of the bonds between molecules. The energy of rotations and vibrations of the molecule is limited to discrete energy levels, making it quantized. When a molecule interacts with radiation that corresponds to one of the discrete energy levels, the radiation is absorbed and the energy state is increased. The implication is that each molecule will absorb very specific wavelengths from a broadband source (Banwell & MacCash, 1994).

Beer's law describes the absorption of light by molecules in its path. The equation below describes transmittance at a given wavenumber, T($\bar{\nu}$), as a relationship between $I_0(\bar{\nu})$ and $I(\bar{\nu})$, i.e. the intensities at a given wavenumber before and after passing through a defined path, respectively. The product of $\varepsilon(\bar{\nu})$, the molar absorptivity coefficient, $\overline{c}$, the concentration profile averaged over the path, and L, the length of the path gives the optical depth, τ, of a given path and relates to the transmittance as follows (Jarvis, 2003).

$$T(\bar{\nu}) = \frac{I(\bar{\nu})}{I_0(\bar{\nu})} = e^{-\varepsilon(\bar{\nu}) \cdot \overline{c} \cdot L} = e^{-\tau}$$

In words, Beer's Law states that transmittance decreases exponentially with increasing concentration, path, and unique absorptivity properties of a molecule. The work in this thesis has been carried out using a spectrometer operating in the infrared region so it will be the focus of this section. Infrared radiation is defined as electromagnetic radiation between 1 μm and 350 μm or 300 THz and 800 GHz. The unit commonly used in infrared

spectroscopy is the previously defined wavenumber (infrared region: 30 cm^{-1} to 10000 cm^{-1}) and will be used exclusively in the remainder of this work. Many of the coupled rotational-vibrational energy modes between atoms of a molecule interact with infrared radiation, provided the dipole moment changes with respect to time during the interaction, as described below.

Vibrations can be symmetric about the center of the molecule, asymmetric, or a bending of particular bonds. Symmetric vibrations do not result in a changing dipole moment, therefore are not infrared active. Asymmetric and bending vibrations do result in a change in the molecule's dipole moment, making them infrared active. The bending and stretching movements of CO_2 are shown in Figure 2.

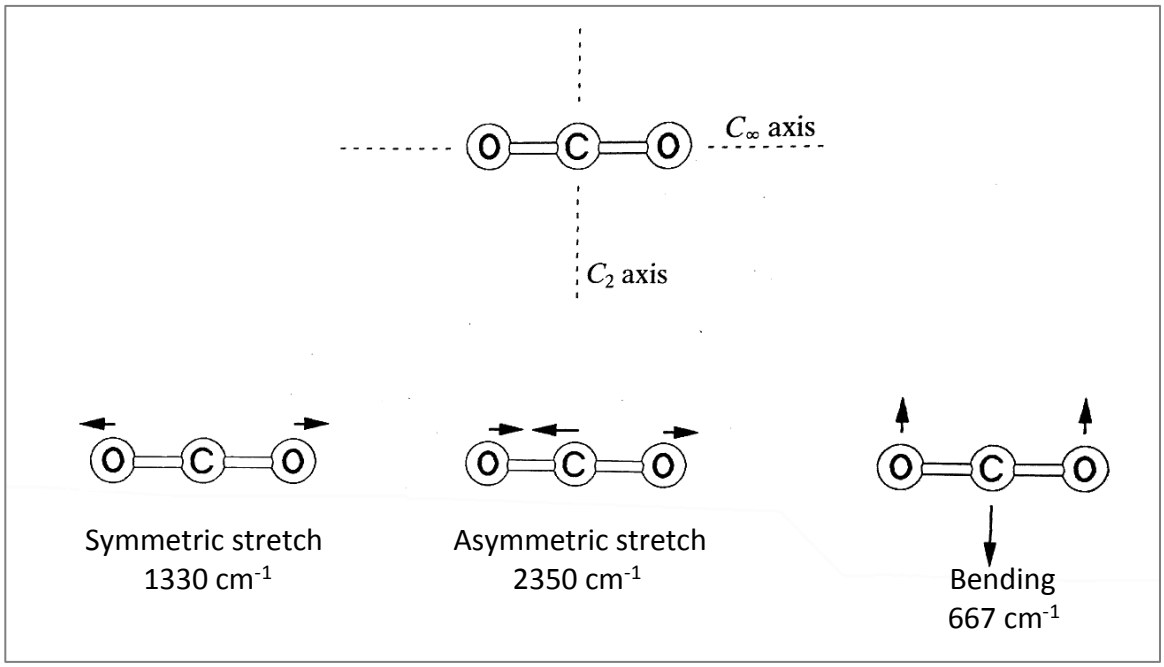

Figure 2: The stretching and bending of CO_2 (Adapted from: Banwell & MacCash, 1994).

The combined vibration-rotation spectrum results in P- and R-branches in the spectrum as shown in Figure 3 that uses the CO_2 spectrum around 2350 cm^{-1} as an example, which corresponds to the asymmetric stretch of Figure 2. The y-axis shows absorbance, equal to the negative logarithm of the transmittance. As such, absorbance tends to zero and infinity when transmittance tends to one and zero, respectively.

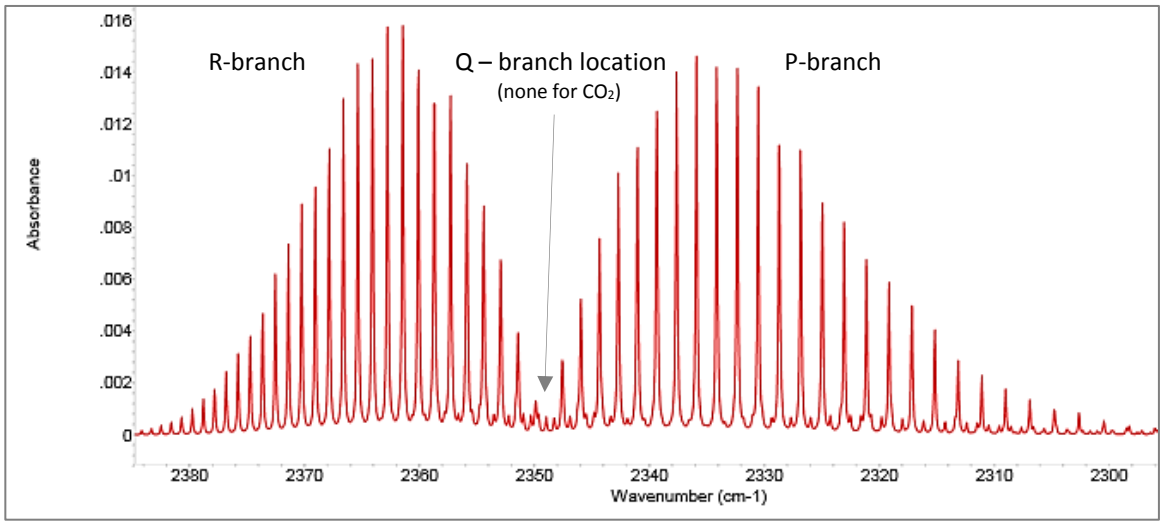

Figure 3: Vibration-Rotation spectra of CO_2 centered at 2350 cm^{-1} for 1 ppm in a 1 meter path at 296 K (PNNL database).

The P-branch lines correspond to changes of vibrational energy with decreases in rotational energy at the same time. The R-branch lines correspond to positive rotational energy changes of state accompanying the vibrational transitions and occur at higher wavenumbers with respect to the central frequency. Each molecule has a set of absorption lines in the spectrum that can be calculated or observed, based on the coupled vibration-rotation mode. The separations of the P-branch lines are larger than R-branch lines due to coupling of vibrational and rotational transitions as well as anharmonicity of the oscillations. A Q-branch line is sometimes located between the P- and R-branch near

the central frequency, forbidden quantum mechanically for this CO_2 stretching mode, and is a result of the rotational number not changing for vibrational transitions from ground state to an excited state in bending modes (e.g. CO_2 at 667 cm^{-1}).

To utilize the absorption spectra of molecules for detection and quantification, the intensity at each wavelength must be determined (Griffiths, 2007). FTIR is an interferometric (as opposed to dispersive) spectroscopic technique, which splits radiation into two and relies on creating an optical path difference in the recombined radiation by sending half of the beam to a moving mirror. The changing optical path difference (OPD) created by the moving mirror results in constructive and destructive interference occurring periodically. The reconstructed beam is focused onto a detector. The output of the detector is therefore the intensity of the signal as a function of mirror position and is referred to as the interferogram. For a monochromatic source, the interferogram would appear as a sinusoidal function of intensity versus OPD. For many wavelengths, from a broadband source, the complex waveform created by the optics in the spectrometer must be separated into its frequency components before gas concentrations can be retrieved. To do this, a Fourier transform is used. This is a mathematical process that transforms the data from a time domain interferogram to a frequency domain spectrum of absorption.

Once the data are in the frequency domain, the intensity at all detected wavenumbers is available to analyse. The spectral range, sampling frequency, and resolution of the data depends on the hardware used for acquisition. The recorded spectra are compared against a set of reference spectra (e.g. Figure 3 for CO_2) using software to iteratively fit molecules and their concentrations to best match the measured spectrum.

1.3. Open Path Fourier Transform Infrared Spectroscopy (OP-FTIR)

One configuration of FTIR spectroscopy is the so-called open-path FTIR technique. An OP-FTIR system records spectra of an active IR source whose radiation passed through an optical path that is in the open atmosphere.

The open-path configuration used at the Tropospheric Remote Sensing Laboratory (TRSL) consists of an active infrared source, spectrometer, telescope, retroreflector, mirror optics, and detectors as shown in Figure 4. The infrared radiation is time-modulated by the spectrometer then collimated using a telescope into a 30 cm beam. It travels typically a few hundred meters through the atmosphere where gas absorption occurs, and is then reflected directly back by a retroreflector. The telescope used for transmission now also receives the radiation and focuses it onto mirrors delivering it to the detector, which records the interferogram, later to be Fourier transformed into a spectrum.

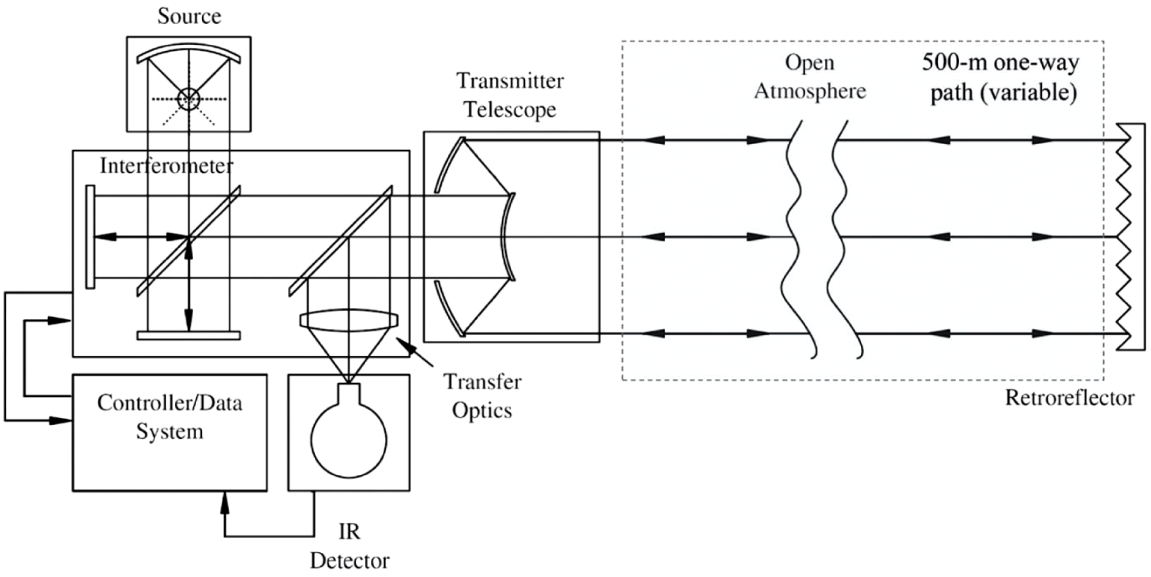

Figure 4: Schematic of a generic OP-FTIR internal and external operation (Adapted from: Jarvis, 2003).

An advantage of the open-path technique is that the long (~400 m) horizontal path provides a larger sample of gas than *in situ* gas sensors, increasing the chance of observing a nearby source. The near-ground-level path also gives a better opportunity to study lower troposphere atmospheric chemistry compared to satellite-based measurement techniques, which have a similarly large footprint.

1.4. OP-FTIR Applications

OP-FTIR technology has been historically used for studying source emissions but is increasingly being used for long term observations due to improved hardware technology and faster, more accurate retrieval software (Griffiths et al., 2009).

The most common use of OP-FTIR is for monitoring emissions from a local source to characterize the species being emitted and their concentrations. Agricultural emissions have been studied within fields used for cattle grazing by monitoring gas concentrations at two different heights over a land area to measure N_2O and Ammonia (NH_3) fluxes (Flesch et al., 2016) and CH_4 fluxes (Flesch et al., 2017). The potential of applying the technology to other flux determination scenarios has been assessed by using up to five different paths to cover the emission area effectively (Hashmonay et al., 2001).

Traffic emissions have also been measured using OP-FTIR, e.g. to characterize traffic emissions on a busy highway exit ramp (Bradley et al., 2000), and to evaluate the impacts of road-noise barriers on near-road air quality (Baldauf et al., 2008), and to evaluate traffic emissions with the path configured to span 16 lanes of traffic across the 401 in Toronto (You et al., 2017), using a very similar OP-FTIR to the one used by the TRSL..

An interesting and well documented application has been to monitor volcanic emissions. The benefits of using OP-FTIR for volcanic emission monitoring is its high accuracy and portability. Campaigns were completed at Masaya Volcano, Erebus Volcano, Stromboli Volcano, and others as a method to monitor the state of the volcano and predict increased volcanic activity, potentially prior to being predicted by seismographs (Horrocks et al., 1999; La Spina et al., 2013; Oppenheimer & Kyle, 2008).

OP-FTIR has also been used to characterize biomass burning emissions from wildfires by calculating emission factors for several species by directly observing the wildfire emission plume (Paton-Walsh et al., 2014). Lastly, OP-FTIR has been used extensively by the TRSL on a campaign basis to study, e.g. shipping emissions (Wiacek et al., 2018), traffic emissions, biogenic emissions, and ambient urban air quality.

1.5. Bruker Spectrometer Design and Performance

The spectrometer used by the TRSL is part of the Open Path System supplied by Bruker Optics Inc., which also includes the telescope and retroreflecting optics as in Figure 5.

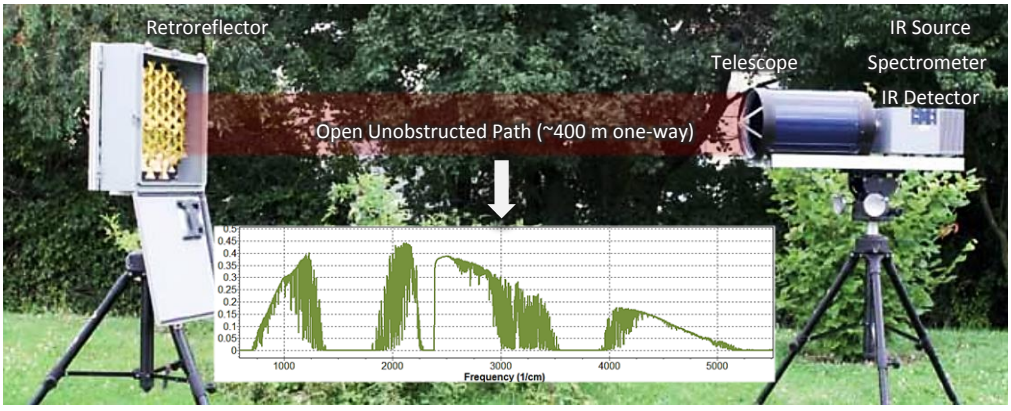

Figure 5: Open Path System by Bruker annotated with a typical recorded spectrum (Adapted from: Bruker, 2013).

This spectrometer's Mercury Cadmium Telluride (MCT) detector is sensitive over a spectral range of 650-5000 cm^{-1} and the interferometer can scan up to 4 times per second at a 0.5 cm^{-1} resolution. An example spectrum is included as an inset in Figure 5 showing typical saturated regions due to water (H_2O) absorption at 1500 cm^{-1} and 3500 cm^{-1}. A Globar™ active source is used in the system, acting as an approximate black body emitter in the infrared region. The emitted infrared radiation is modulated by a RockSolid™ interferometer, using two cube corner mirrors and a beamsplitter, and passed through another beamsplitter on its way to the telescope (Figure 6). The modulated radiation is collimated into a 305 mm (12") beam by a modified Schmidt-Cassegrain telescope as it exits the spectrometer. The radiation travels externally to the retroreflector about 400 m away, depending on the application. A retroreflector is an array of cube corner mirrors (Figure 5) that reflects the beam of radiation directly back along its incident path. The same telescope used for the transmission then receives the radiation, diverting it to a detector through the second beamsplitter, now encountered first. A focusing mirror bends the radiation onto the MCT detector. To minimize thermal noise in the detector, a Stirling cycle cryo-cooling system reduces the temperature of the detector element to 77 K. This method is beneficial over the more common use of liquid nitrogen for cooling as it eliminates the complication of refilling the detector dewar in the field. The received signal will contain some amount of stray light emitted from external sources, which adds to the signal. This stray light signal can be removed since the source radiation was modulated at approximately 1 kHz before it was transmitted out of the spectrometer, making it possible to filter the atmospheric emission spectrum because it is comprised of unmodulated stray

light. The interferogram is recorded in the time domain by a laptop computer that controls acquisition (not shown) and also performs the fast Fourier transform on the interferogram to generate the spectrum. Spectra are calculated and stored once every minute (adjustable depending on application) by the acquisition laptop.

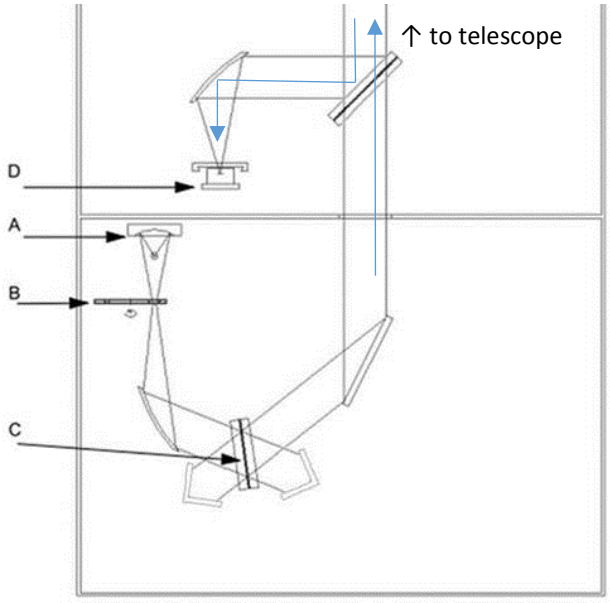

Figure 6: Internal optics of the Bruker OP-FTIR showing A) infrared source, B) aperture wheel, C) beam splitter, and D) detector (Peter Maas, personal communication, November 2017).

The spectrometer is designed for quick and easy setup in the field for studying emission sources and events with chemical signatures in atmospheric composition. While this process is relatively uncomplicated, it does require training with the equipment for both setup and operation. A Standard Operating Procedure (Appendix A: OP-FTIR Standard Operating Procedure) was created as part of this work to guide users with equipment setup and data acquisition, beyond basic instructions provided by the manufacturer, including detailed instruction on setup, software use, and periodic maintenance.

1.6. Scope of Work

The Tropospheric Remote Sensing Observatory currently under construction at Saint Mary's University is filling a measurement gap both geographically and in terms of providing the first continuous measurements of VOCs. These boundary layer measurements of VOCs and other air quality and climate relevant trace gases are also expanding the scope of use for OP-FTIR technology, which has to date been deployed on a campaign only basis.

The rest of this thesis documents the design of the shipping container-based TRSL trace gas observatory and the work completed to automate weather protection of the OP-FTIR system that is currently its central instrument (Chapter 2). A a case study of the detection of biomass burning emissions with the OP-FTIR instrument while deployed on a campaign-basis at SMU (Chapter 3) documents instrument performance in one future application of the TRSL, i.e., the continuous detection of VOCs and other trace gases related to multiple emission sources impacting Halifax air quality. Finally, Chapter 4 outlines future work remaining in order to complete and fully automate the Tropospheric Remote Sensing Observatory at SMU, as well as suggestions for improving the biomass burning emission detection study.

2. Observatory Design and Automation

The TRSL has a goal of near-continuous monitoring of trace gas concentrations in Halifax. A dedicated OP-FTIR observatory is a world first and will result in unique datasets for use in atmospheric science research in Halifax. The dataset will also be relevant to other locations with similar geography and aid satellite validation in a coastal environment.

The OP-FTIR requires a completely open atmospheric path for operation because infrared radiation is absorbed by most glass and plastics that could be used as economical windows. Infrared transmissive crystals are prohibitively expensive in the 30 cm diameter required, and they experience serious degradation in the open atmosphere. At the same time, the OP-FTIR has sensitive parts that could be damaged by the harsh climate of a coastal city that experiences winter or high humidity conditions for large parts of the year.

To achieve the observational goal of the TRSL while protecting the instrumentation being used, a new observatory has been designed as part of this thesis work and will be installed at SMU. The observatory features a 24’ by 20’ tiled rooftop working space for atmospheric measurements, with partially automated environmental protection in place.

2.1. Detection Limits and Path Length

The design of an observatory with the OP-FTIR as the primary instrument must consider the available optical paths from the location to potential retroreflector locations, which will affect the detectability of trace gases of interest were examined. For a molecule to be detectable using OP-FTIR it must meet several conditions including 1) absorbing in the detection range of the hardware, 2) absorbing in a region of the spectrum not saturated

by another gas, and 3) having a sufficient concentration or absorption strength so as to have quantifiable absorption signatures in the spectrum.

The OP-FTIR manufacturer provided detection limits for a number of trace gases based on the largest absorption feature of each gas being three times the noise level in a spectrum with a 450 m two-way path, co-added from 240 interferograms over 1 minute. This is useful for approximating if a gas will be detectable but requires more information about a typical ambient concentration of the gas and the measurement conditions, in case ambient levels are much lower than the detection limits.

A major factor of detectability is path length, as a longer path results in more of the target gas in the path. This is also a factor that is controllable during the measurement stage. To guide the design of the observatory and to aid in future measurement campaigns and retrievals of gases, a trace gas information database was created detailing expected detection capabilities versus path length. The database (Table 1) can help a user plan a measurement campaign or decide if a certain trace gas retrieval is viable for a past campaign, where path length cannot be changed. Trace gases for which the ambient level is near the Bruker supplied detection limit should be closely scrutinized when attempting to measure or perform retrievals. Approximate path lengths that result in a peak absorption of 0.5% by the molecule were simulated using the Multiple Atmospheric Layer Transmittance (MALT) model software. Through experience and research, this level of absorption should yield a retrieval with a sufficiently stable fit because it corresponds to three times the noise levels found in our typical spectrum. Also note that all simulations were completed for typical summer conditions with a temperature of 25 ˚C, a pressure of

1013 mb, and 1% water vapor concentration. Water is a strong absorber of IR radiation in many spectral regions and is a major factor for limiting retrieval possibilities. In the winter, when the air typically contains less water, trace gases are easier to retrieve because their absorption features stand out more in spectra.

Table 1: A selection of trace gases with detection limits and absorption simulation results at typical one-way paths. Path for percent absorption scales linearly (e.g. for 1% absorption the path will double).

Trace Gas	Ambient Concentration [ppb]	Retrieval Windows [cm^{-1}]	Bruker Limits [ppb]	Peak Absorption Percent @ 350m	Path for 0.5% Absorption [m]	Interfering Gases
CO_2	~400000	2030-2133	133.32	100	Any	H_2O, CO
CO	~50-120	2080-2133	1.38	10	Any	H_2O, CO_2, N_2O
CH_4	~1800	2900-3024, 1250-1300	1.42	89	Any	H_2O
CH_3COOH	4.4	1130-1230	1.23	0.05	400	H2O, HCOOH
CH_3OH	1	1020-1063	1.29	3.60	Any	H2O, CO2, O3, NH3
NH_3	10	920-1044	1.06	2.00	100	H_2O, CO_2, CH_4, C_2H_4
H_2CO	2	2720-2846	1.98	0.13	>800	H_2O, CH_4
C_2H_6	4	2976-2987	1.55	1.60	425	H_2O, CH_4
HCN	1	3268-3360	3.63	0.36	400	H_2O, CH_4

While increasing the path length can improve the detection limit of some trace gases, there is a trade-off with the reduction of return signal strength. Figure 7 is a plot showing a comparison between two-way path length and the peak signal level in the spectrum of the returning radiation. Similarly, Figure 8 shows the effects of increasing path length as measured by Bruker. The reduction in signal strength is due to the divergence of the beam such that the growing area of the beam with distance overfills the retroreflector and not all radiation is reflected back to the spectrometer. The divergence has been determined

experimentally to be approximately 2.7 mrad. Peak signal data comes from previous campaigns performed by the TRSL and is influenced by other factors such as quality of the alignment and fog. The result is ideally to increase the path up to the point where the signal begins to degrade quickly. A two-way path of ~600m is recommended.

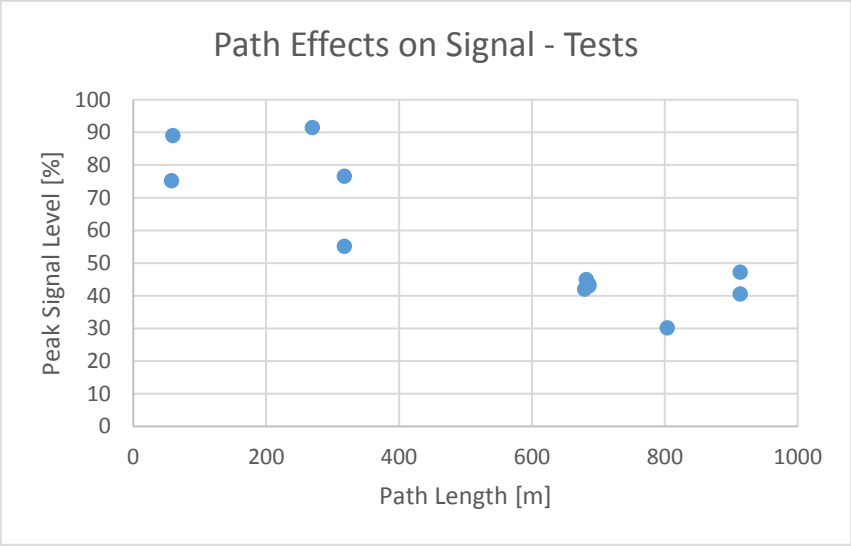

Figure 7: Two-way path length versus peak signal in received spectra with best fit.

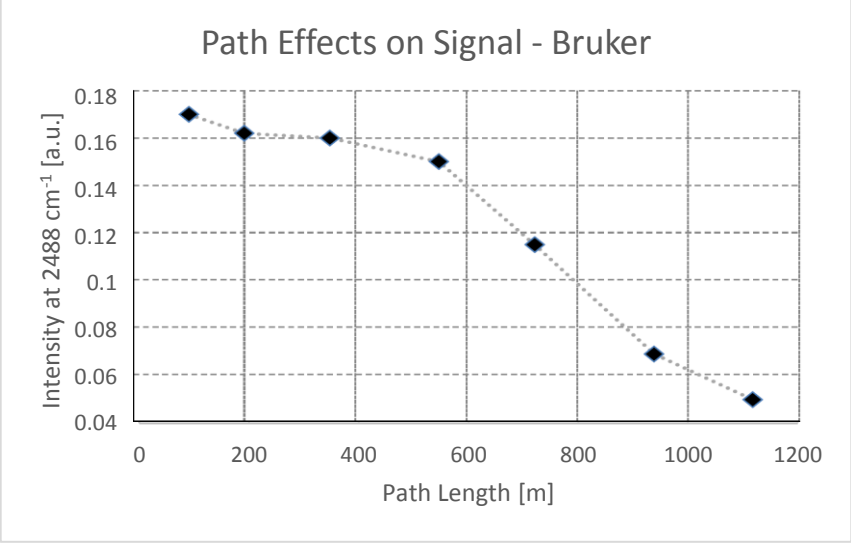

Figure 8: Bruker supplied intensity versus two-way path length (Adapted from: Bruker, 2015).

2.2. Spectrometer Enclosure

The spectrometer is the main component of the OP-FTIR, consisting of the infrared source, beamsplitter, mirrors, interferometer, telescope, and detectors. The laptop that controls the spectrometer acquisition and stores the measured spectra is co-located with the spectrometer. The spectrometer will be located in a newly designed and purpose built observatory on the top of the Student Centre Building. The design process for this observatory involved many iterations that considered both the Group's research goals as well as the university Facilities Management constraints in making the observatory a structural part of an existing building.

The minimum observatory requirement is that of a space with adequate accessibility for operation and maintenance as well as sufficient sightlines to other accessible locations to place retroreflectors. The sightlines are critical to the operation of the equipment, as the path length determines detection limits. The sightlines will ideally lie between 200 m and 400 m to allow retrieval of many target trace gases, while not over or under filling the retroreflector significantly.

Initially, the use of a space on top of the McNally building was explored, followed by the Science Building and the Atrium. The final location was chosen as the Student Centre Building, which is near the centre of campus at a high (~60' = 18m) vantage point with several sightlines to other buildings. It meets the structural requirements, as verified by Facilities Management and their engineering consultants. Figure 9 shows the location where the observatory will be installed, while Figure 10 shows this location from above with sightline availabilities shown and path distances overlaid as circles. Targets exist in

our ideal range to the South, on campus, while other suitable locations lie on private property and will require permission to install a retroreflector. The currently available campus positions on the Rice and Loyola Building rooftops will be used with the possibility of adding other locations in the future.

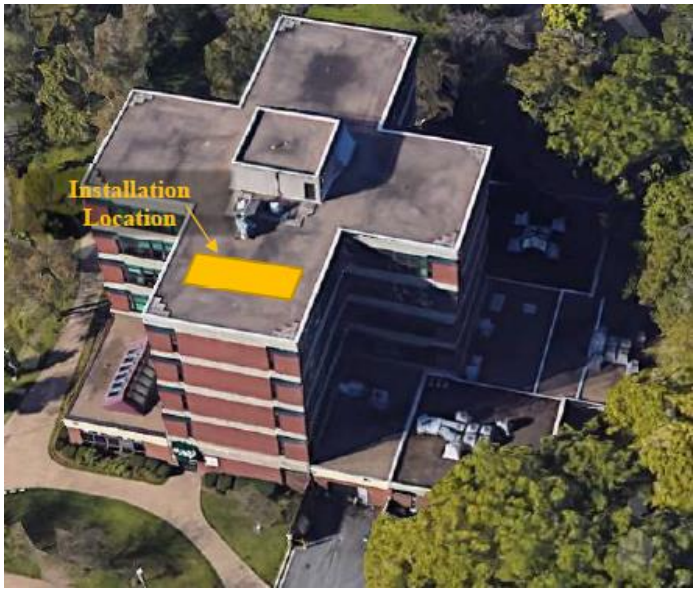

Figure 9: Observatory Location on the Student Center Building at SMU, adapted from Google Maps, 2017.

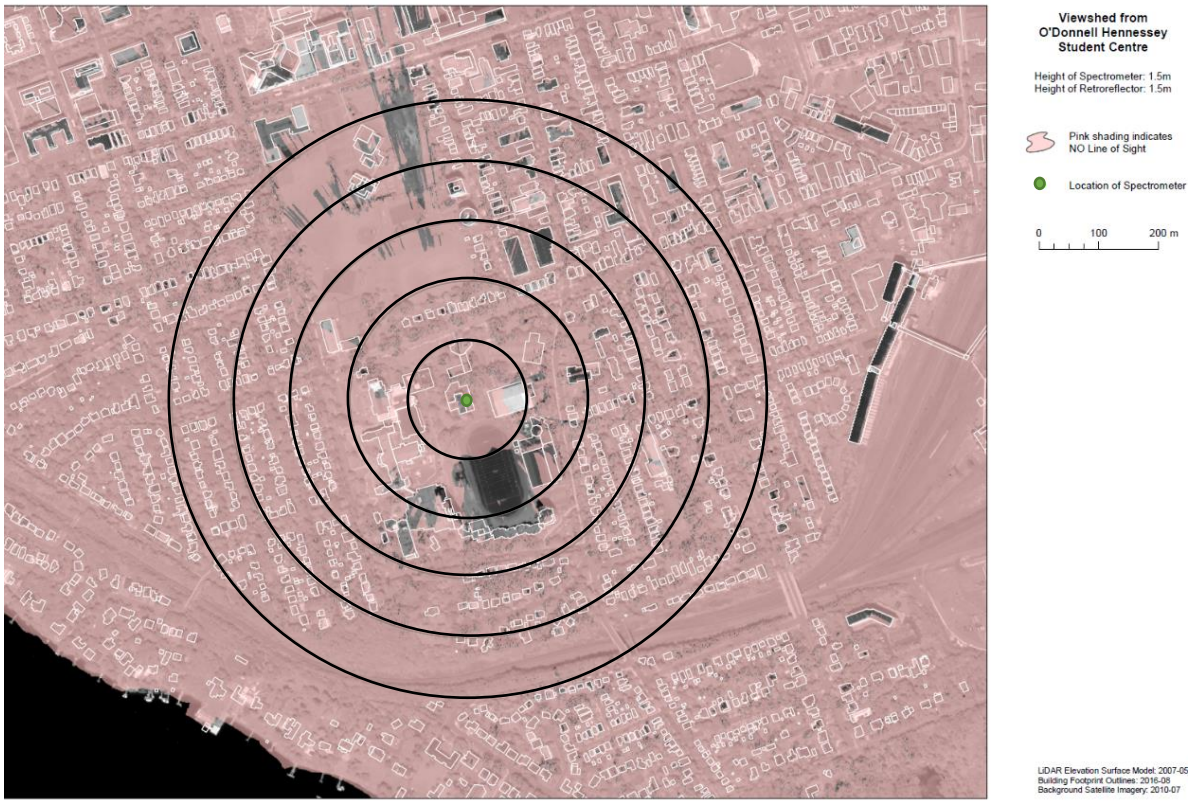

Figure 10: Viewshed from observatory, indicating suitable retro locations (Courtesy: Greg Baker, SMU).

The observatory was designed to accommodate the OP-FTIR and also provides space for additional future atmospheric measurements by the TRSL and other researchers, e.g. an ultraviolet open-path system, aerosol measurements, and boundary layer measurements. The observatory will be based on a shipping container structure because they are highly customizable and portable via cranes and flatbed trucks. Containers have been used extensively in the NDACC/TCCON atmospheric observing networks (Geibel et al., 2010), as well as in oceanic research (Dalhousie University News, 2017).

The design includes six awning windows that open to a minimum of 90^{o} for taking measurements with the OP-FTIR, a mast for wind monitoring, ample power (up to 12 kW) for equipment, and rooftop goosenecks for the addition of other atmospheric equipment,

which may require power or gas inlet tubing to pass between inside and outside. A roof hatch and exterior rooftop ladder has been included, anticipating future measurement needs of the zenith sky or of a tracked solar beam. The proposed schematic and renderings created for the observatory project as part of this work are shown in Figure 11 and Figure 12. The interior has evenly distributed lighting, several power outlets (including 220 V for possible larger equipment), and data ports. There is an HVAC (heating, ventilation, and air conditioning) unit to maintain an acceptable climate for the equipment. Part of this work included being involved from start to finish in creating a request for proposal (RFP), the scope and minimum requirements of which are included in Appendix C: Observatory RFP.

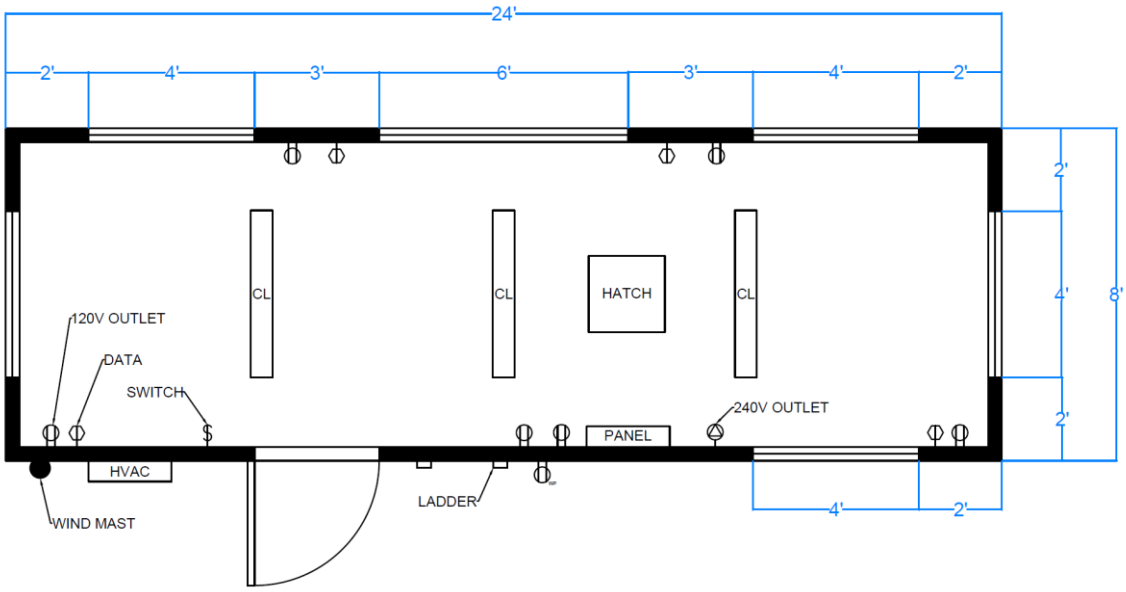

Figure 11: Proposed observatory schematic.

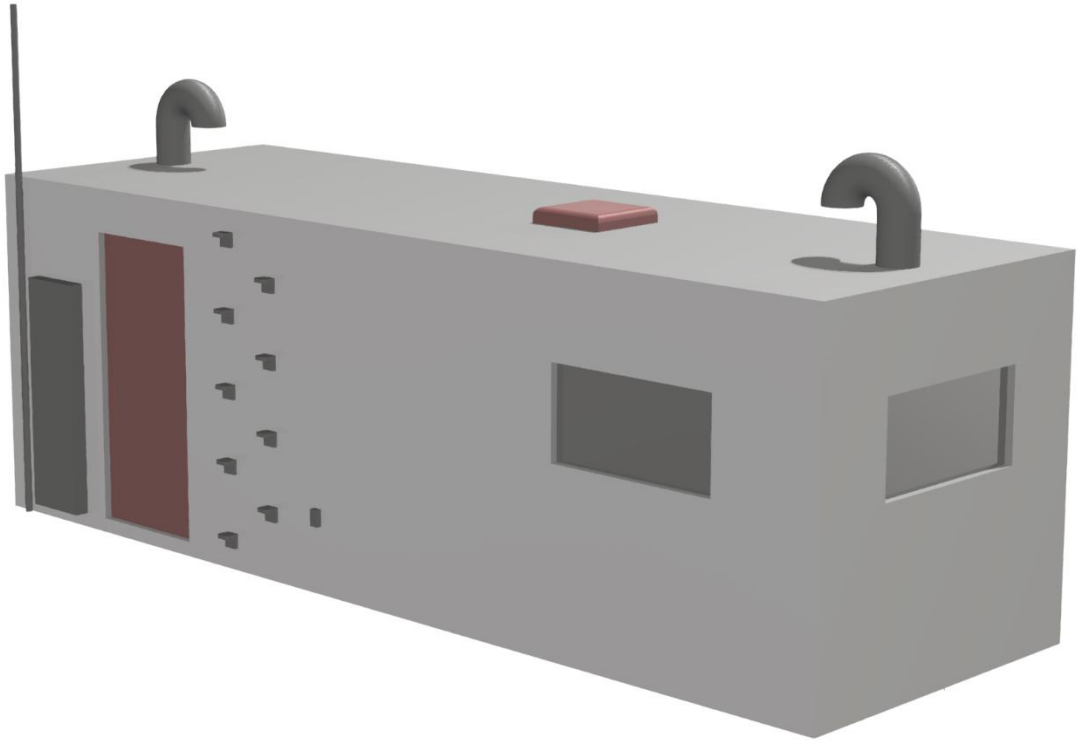

Figure 12: Rendering of observatory (wind mast not to scale).

Placement of windows is critical to the operation of the observatory because they dictate the available sight lines to potential retroreflector locations. The spectrometer is mounted on a tripod and automated pan/tilt head that has a minimum height it can be lowered to. The tallest building on SMU campus is the Loyola Building and it is a potential target for a retroreflector because of its fenced in, parapeted, and fairly accessible rooftop. The windows in the observatory must be placed high enough so the spectrometer has a full line of sight up to the Loyola rooftop. The relative heights and horizontal distance of the spectrometer and retroreflector were compared to find the vertical angle between them, then the geometry of the spectrometer was used to find the window height, accounting for the spectrometer being placed 1’ away from the window and the awning being open to 90° as in Figure 13.

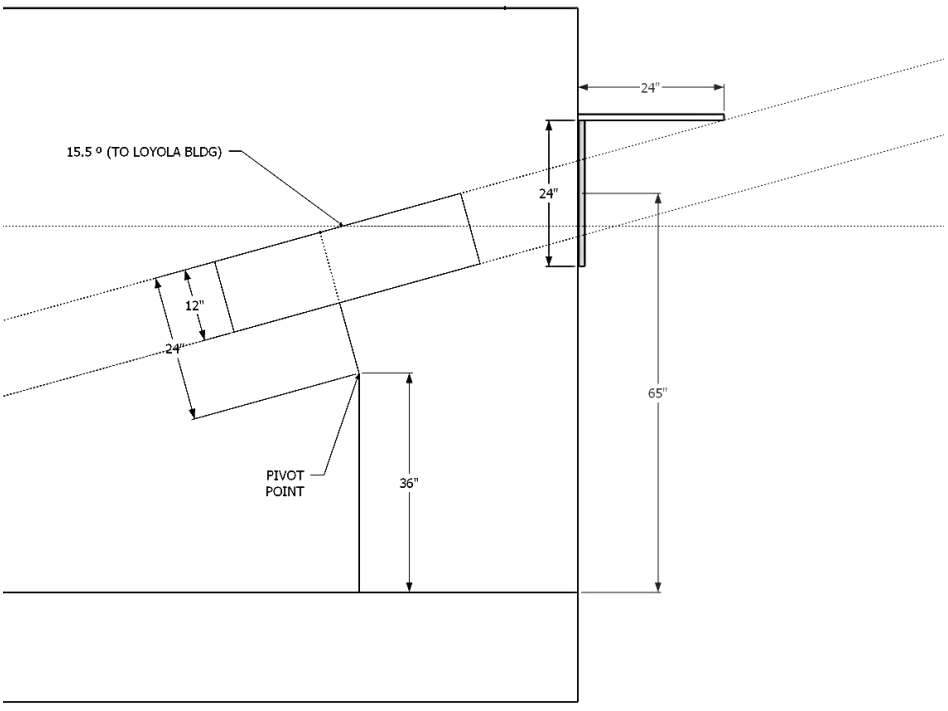

Figure 13: Window vertical placement model, showing minimum 65” window center from floor.

After securing financial backing from the university, the RFP was posted for companies to bid on the contract to construct the observatory. Another aspect of this work involved judging the proposal submissions prior to contract award. Facilities Management has also moved forward with modifying the rooftop so the observatory can be installed. The modifications involve building a frame to secure the observatory to the rooftop and an additional roof drain to prevent water from pooling on the roof. Additionally, railings will be installed between the mechanical penthouse and the container sides to allow safe access by researchers and students (Figure 14). The current schedule has the observatory built and installed on the rooftop, ready for use, by mid-June.

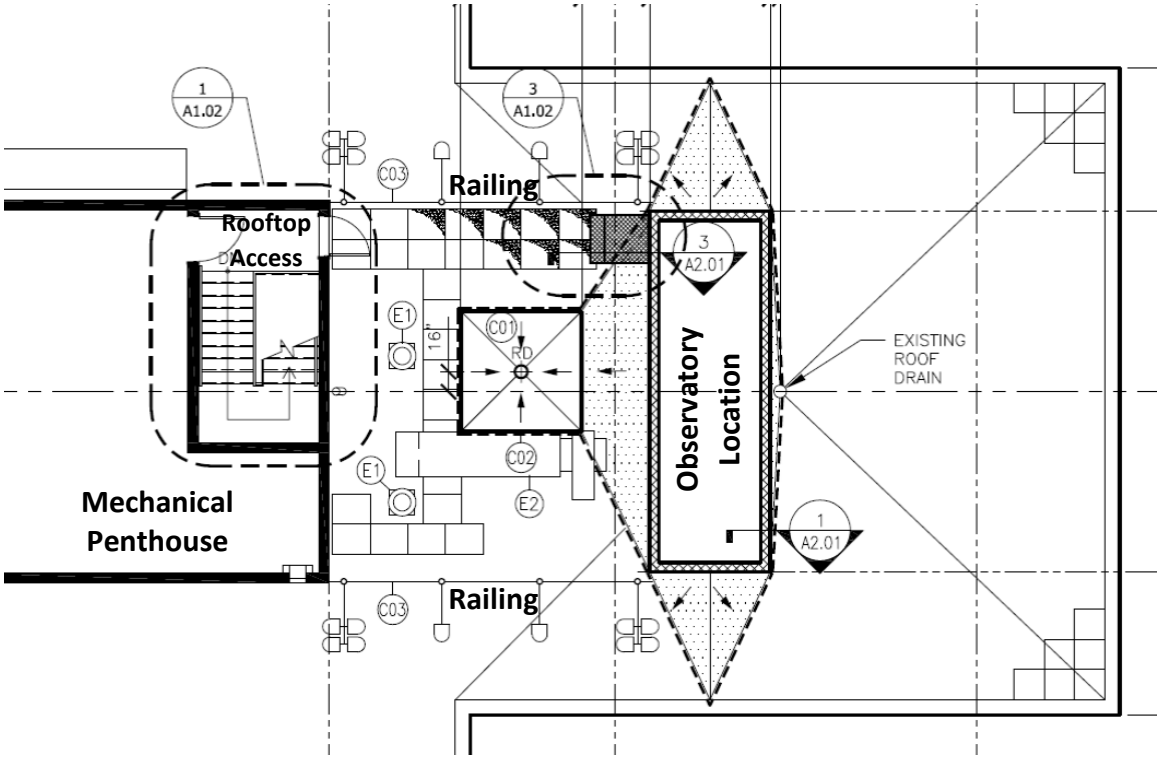

Figure 14: Student Center Building rooftop modification plans (Barry McNeil, personal communication, March 2018).

2.3. Retroreflector Enclosure

Located a few hundred meters away from the main observatory is a retroreflector. The array of gold coated cube corner mirrors is susceptible to wear and damage from environmental factors if exposed for long periods of time. The array is mounted in a metal box measuring 26”×26”×8” that is rated to NEMA 13. The NEMA rating means that when closed, it is resistant to the ingress of dust and low-pressure streams of water from any direction. It is not desirable to have someone manually access the retroreflector to close it in every case of bad weather because it would likely lead to some periods of exposure to extreme conditions and/or lost measurements during times of good weather. The solution to this is to have a method of opening and closing the NEMA rated box remotely, and even autonomously. To achieve automation of this process, a method of opening the heavy steel retroreflector door upwards is required, along with wireless communication over several hundred meters, and a weather reactive program that runs continuously. The exact components chosen and used for this project are listed in Appendix E: Observatory Automation Solution Parts List so that any future problems can be more easily found and parts fixed or replaced.

Linear actuators were chosen to open and close the NEMA box door. Linear actuators are capable of outputting large forces with relatively small power consumption (several amps). They operate via an electric motor and then convert the rotational movement into linear displacement, causing an actuating shaft to move in or out. A design with two actuators, one on each side, was chosen to provide sufficient power, applied evenly across

the door. Force calculations were performed and a factor of safety was applied, the details for which are supplied in Appendix D: Retroreflector Door Force Requirements.

A steel bar was affixed to the door with actuator mounts on each end. Actuator mounts were also added to the modular aluminum frame of the retroreflector housing. The result, both in the closed and open state, can be seen in Figure 15. The original pneumatic lift assist was left on the inside of the NEMA box door to aid in the lifting of the door and add support, as it does in manual use. The actuators are attached to the mounts using shafts with hairpin cotter pins (R-clips) so they can be easily removed in the event that they are stuck in the up or down position. Protection against single actuator failure, which would result in damage to the box in the form of strong twisting of the door, was added by putting 1.25 A fuses (chosen from load-current testing) in-line with each actuator. The failure of one actuator will result in an increased current in the other, as it works to overcome the holding force of the failed actuator, therefore blowing the fuse and stopping motion and damage.

Figure 15: Retroreflector housing fitted with actuators in closed (left) and open (right) position. Red arrows indicate linear actuators.

The actuators need to be controlled remotely, from the observatory or from a remotely connected computer. Relays are often used to control the power and direction of actuators. They allow the high current of the actuators to be controlled by a smaller current produced by a computer or microcontroller. For the communication, radio frequency (RF) is often used for a medium range communication requirement such as this one. An off-the-shelf solution was found that consists of an RF transmitter and receiver already fitted with the appropriate relays. The RF controller states an operation range of up to one kilometer over an unobstructed path. RF controllers can be susceptible to interference by other devices operating on the same frequency (315 MHz), if this occurs the code should be changed on the receiver and transmitter as per the device's manual. To power the retroreflector door control solution, a 12 V power supply is required as the RF controller and actuators operate at this voltage. This has been supplied in the form of a power supply (12.5 A max) that can be connected to building power for long term use, or a battery that allows the system to operate fully wireless for up to two weeks under normal use. This two week figure comes from the battery size (7.2 Ah), the draw in standby mode (11 mA), and the draw during movement (1.5 A); resulting in 27 days of standby or 300 cycles of open or close, for a combined conservative estimate of two weeks under normal operation. The solution was wired together with quick connect fittings so the system can be assembled and disassembled easily. The electrical diagram in Figure 16 gives an overview of the solution and how it is wired together (transmitter wiring shown separately). The retroreflector opening and closing was tested using the RF

transmitter with success over a 350 m distance in 2017 summer conditions and 2018 winter conditions.

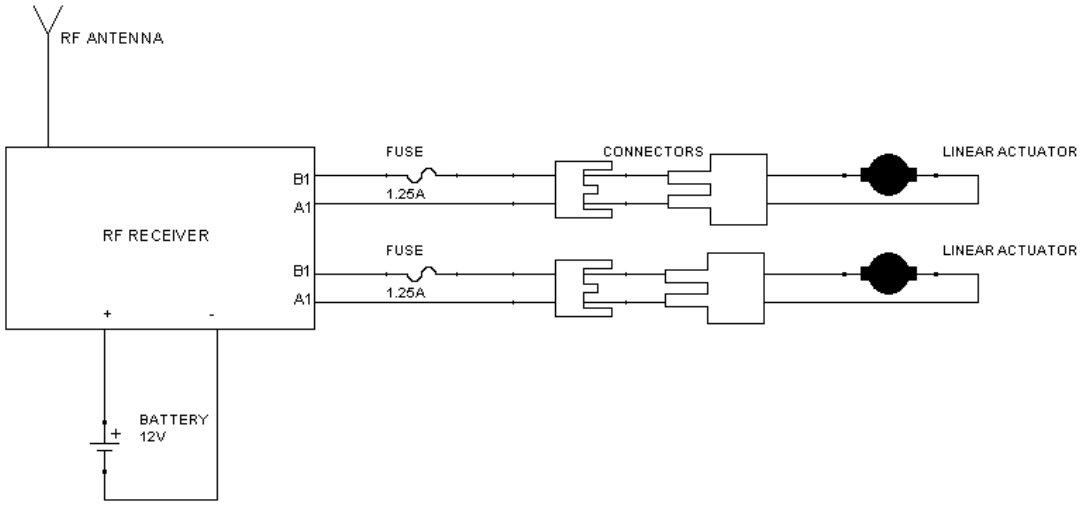

Figure 16: Retroreflector housing receiver-side door control electrical schematic.

2.4. Automation

Weather is constantly changing, and the equipment must be protected from heavy rain, strong wind, snow, and ice pellets all while measuring data when these conditions are not seriously impacting the OP-FTIR signal levels and putting the equipment at risk of exposure. Sources of reliable weather data near SMU were identified as a Davis Pro II weather station along with a cloud and precipitation sensor, both located on top of the McNally building and shared by the Environmental Science and Astronomy and Physics departments. The weather station provides current data through Weather Underground (https://www.wunderground.com/personal-weather-station/dashboard?ID=INOVASCO115) including current conditions (e.g. clear, rain, snow, etc.), precipitation rates, and wind

speeds. UV irradiance and solar flux data indicative of photochemical activity are additionally provided by the Davis Pro II, but are available from the Burke Gaffney Observatory (BGO) dash board. The cloud and precipitation sensor is an extremely reliable sensor operated by the BGO (https://www.ap.smu.ca/~bgo/cloud/) that is used to make decisions to close the astronomical observatory dome to protect the telescope from any precipitation. The sensor provides four states of conditions: “clear”, “cloudy”, “very cloudy”, or “wet”. The combination of these two data sources can be used to make informed decisions about the current state of the weather at the observatory, and consequently whether to record data or close the retroreflector housing.

The code currently closes the retroreflector enclosure when winds exceed 50 km/h, rain exceeds 0.5 mm/hr, the conditions are ‘rain’, ‘ snow’, ‘hail’, or ‘freezing’, or when the BGO sensor reports ‘wet’. These conditions can be easily changed for more or less aggressive weather protection.

The RF transmitter that sends signals to the retroreflector door actuators consists of a remote control with several buttons (out of the box). It is desirable that a laptop is used for sending the signals rather than human input via remote control button pushes, so a method of interfacing the laptop to physical voltage outputs needed to be found. A board called the Numato USB to GPIO (General Purpose Input Output) was chosen to solve the interface problem. This board connects to a computer via USB and appears to the computer as a serial output with 8 lines. These lines translate to 8 relays that are open when the corresponding output is off and closed when the output is on. Three of these relays need to control the three buttons on the remote, one for up, one for down, and

one for stop. The positive and negative of each button can be connected to the common and normally closed outputs of a relay. Figure 17 shows an image of these components wired together and Figure 18 shows an electrical diagram of the solution.

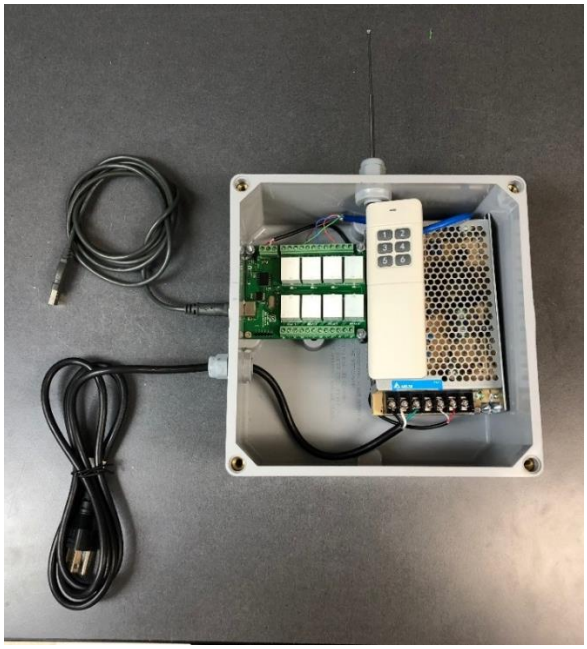

Figure 17: The USB to GPIO board wired to the RF transmitter.

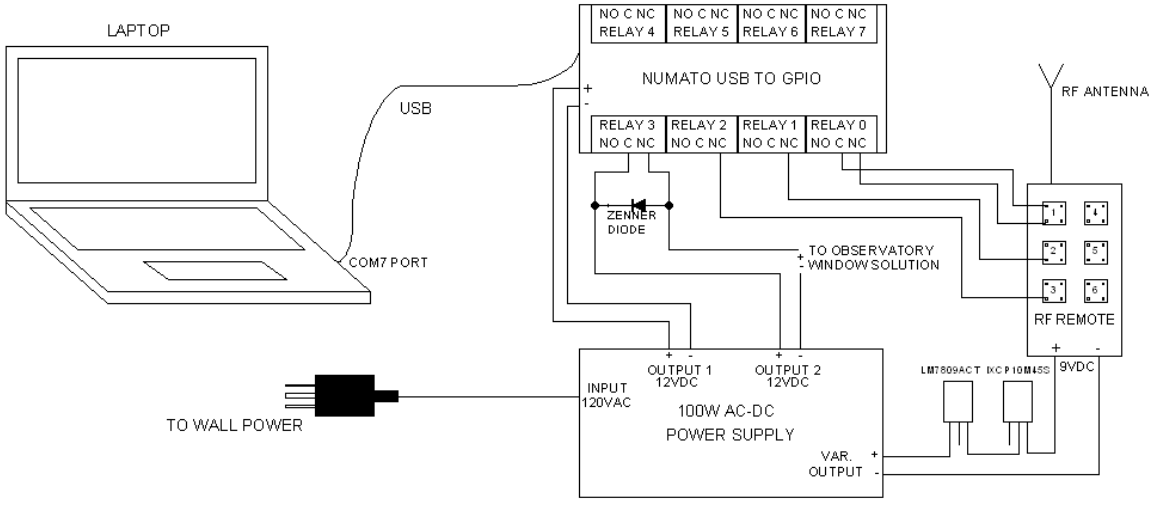

Figure 18: An electrical diagram of the laptop to RF transmitter interface on the transmitter side.

Once input variables from the weather stations and output variables to the GPIO board have been identified, a software solution was used to link them together. Python was chosen as the programming language because it is robust and commonly used for similar applications. Python was used to scrape data from the websites run by Weather Underground and the BGO. This data was then used in a decision-making algorithm about the state of the weather. The decision results in a call to send out the appropriate serial output to the USB to GPIO board, leading to the appropriate action of the retroreflector enclosure, i.e. either to open or close. A GUI (Graphical User Interface) was added to allow monitoring of the current weather conditions, manual override of the automated open/close decision, and error messages in case of lost connection to weather websites or GPIO board. The code is found in Appendix F: Weather Control Python Script and a screenshot showing the GUI is shown in Figure 19. In testing, the software performs well, however sometimes experiences errors that result in it “not responding”. Additional work should be completed improving the stability of the software by utilizing exception handling.

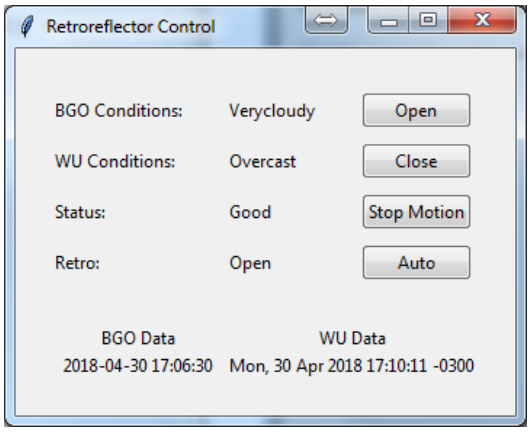

Figure 19: GUI of retroreflector control program with weather status (Good/Bad), retro door status (Open/Closed), and action buttons on the right to override the algorithm's decision.

2.5. Path Bending Flat Mirror

As discussed in previous sections, path length is an important consideration when attempting retrievals of low concentration gases. Physical restrictions such as unavailability of space in suitable locations may prevent a desirable path length from being attained. Another problem associated with a straight path length is the bias resulting from the wind being along or perpendicular to the observation path. One solution to these is the addition of a flat mirror into the path. Several configurations are possible with this addition, some of which are shown in Figure 20. Configuration A doubles the path while keeping the spectrometer and retroreflector locations the same. Configuration B reduces wind direction bias by creating a path in which one half is perpendicular to the other half. The concept of adding this mirror has been tested in an agricultural study where the bent path was used to better encircle a field successfully (Flesch et al., 2016).

The flat mirror needed to be extremely reflective in the same infrared region that the OP-FTIR operates in to minimize loss of signal, and be sufficiently large so that the entire 30 cm diameter beam is reflected. The chosen mirror was purchased from Edmund Optics (Stock #85-207) and meets the infrared criteria by having a 4-6 λ flatness (typical grade) with a size of 408 x 609 mm. A tripod was purchased from Manfrotto (Part #: 058B) with the head (Part #: 405) for aiming the mirror to align the infrared beam. A mount for the mirror was constructed using plywood painted with exterior water seal paint and aluminum angle bar to secure the mirror, as shown in Figure 21.

Figure 20: Path extending flat mirror configurations.

Figure 21: Flat mirror, mount, tripod head, and tripod.

The mirror was tested in the lab to find the actual reflectance. Two optical paths of identical total length were setup, one including the flat mirror and one without it. The peak infrared signal was compared between these two paths and it was found that the reflectance of the mirror was 86%. This is lower than the quoted typical value above 95% for protected aluminum from the manufacturer. This results in a 74% reflectance in practice, or 26% signal loss, because the signal must reflect off the mirror twice in traversing the total optical path. The loss of signal should not be a serious problem for regular measurements but it means that in degrading conditions such as fog the signal will become attenuated beyond a useful level with lower degrees of weather degradation. The next step for this project is to test it in the field in multiple configurations, starting with an orthogonal path (configuration B).

3. Biomass Burning Case Study

The OP-FTIR was deployed on the SMU campus during two biomass burning events in 2016 with the goal of characterizing the detectability of the events in Halifax, NS using trace gas fingerprinting based on emission factors and atmospheric transport modeling. One of the events was a large wildfire which occurred in Fort McMurray, Alberta (AB) 1300 km away from Halifax and the other was a much smaller wildfire that occurred near Seven Mile Lake, NS 130 km west of Halifax. Previously, large boreal fires have been detected far down stream with similar technology (Franklin et al., 2014). Table 2 outlines the fire descriptions, burn dates, and OP-FTIR measurement data available. The overall approach was to identify trace gases that are good tracers of biomass burning emissions, to retrieve their concentration time series, and to attempt to correlate concentration enhancements with likely times of emissions transport from wildfire regions, as identified with transport trajectory modeling.

Table 2: Biomass burning event locations, sizes, and temporal burn ranges (in 2016).

Fire	Location	Size [ha]	Burn Dates		Measurement Dates	
			Start	End	Start	End
Fort McMurray, AB	56.63N 111.31W	423000	May 1	July 4	May 5	May 25
Seven Mile Lake, NS	44.51N 65.27W	367	August 3	August 15	August 9	August 15

3.1. Biomass Burning Tracer Gases

The OP-FTIR was setup and recorded spectra for the longest duration possible during each of the biomass burning events, given weather and logistic constraints. A selection of trace gases was chosen as biomass burning tracers based on their infrared activity and measured emission factors from wildfires (Akagi et al., 2010), as shown in Table 3. The emission factors give grams of tracer gas emitted per kilogram of fuel burnt. The main products, by mass, are CO_2 and CO, as expected, with much smaller quantities of other minor tracers. It must be noted that some tracers are not unique to wildfires and others are only marginally detectable.

Table 3: Trace gases used as tracers of biomass burning.

Trace Gas		Retrieval Window [cm^{-1}]	Interfering Gases	Emission Factor [gkg^{-1}]
Carbon Dioxide	CO_2	2030-2133	H_2O, CO	1489
Carbon Monoxide	CO	2080-2133	H_2O, CO_2, N_2O	127
Methane	CH_4	2900-3024, 1250-1300	H_2O	5.96
Acetic Acid	CH_3COOH	1130-1230	H_2O, HCOOH	4.41
Methanol	CH_3OH	1020-1063	H_2O, CO_2, O_3, NH_3	2.82
Ammonia	NH_3	920-1044	H_2O, CO_2, CH_4, C_2H_4	2.72
Formaldehyde	H_2CO	2720-2846	H_2O, CH_4	1.86
Ethane	C_2H_6	2976-2987	H_2O, CH_4	1.79
Hydrogen Cyanide	HCN	3268-3360	H_2O, CH_4	1.52

The trace gas data was collected on SMU campus, oriented as in Figure 22 with the spectrometer in the Science Building aiming out of an open fourth floor window and the retroreflector on the rooftop of the Rice Building, with a total optical path of 686 m. The

spectrometer was operated in its usual setting of 0.5 cm^{-1} resolution, co-adding 240 interferograms to produce one spectrum per minute.

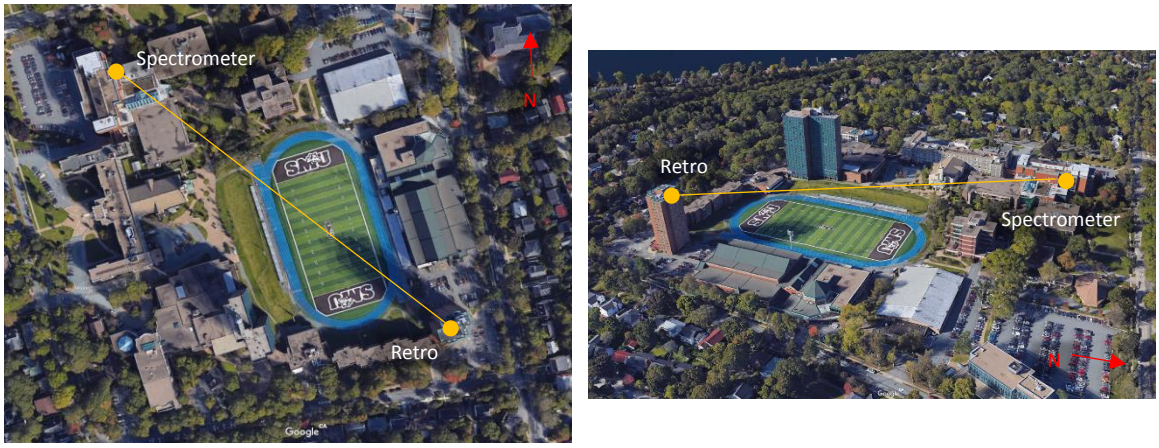

Figure 22: Orientation of OP-FTIR during biomass burning event measurements.

3.2. Transport Modeling of Biomass Burning Emissions

Transport modeling is a useful tool in atmospheric research to identify general movements of air masses over short to long distances. Transport of theoretical "particles" released to the atmosphere is primarily governed by wind speed, among other meteorological factors. The Hybrid Single Particle Lagrangian Integrated Trajectory Model (HYSPLIT) is an atmospheric transport model that calculates such "particle" trajectories and dispersion concentrations (Stein et al., 2015).

The first step in making accurate transport calculations is to identify the times and locations of the emission sources that are the target of the transport study. Fire data was taken from NASA's Fire Information for Resource Management System. The data consists of satellite observed mid-infrared and thermal infrared brightness temperatures with one kilometer resolution, derived from both the Moderate Resolution Imaging

Spectroradiometer and the Visible Infrared Imaging Radiometer Suite instruments (Jackson et al., 2013; Remer et al., 2005).

The cumulative fire counts for each fire over the duration of their active burning time is shown in Figure 23. A rectangle showing the chosen trajectory starting region for each event is overlaid.

Fort McMurray, AB

Annapolis Valley, NS

Figure 23: Fire counts and estimated emission area in 2016 biomass burning case study.

To model the NS wildfire emissions, initially a matrix of trajectory start points was placed in the chosen area. This approach did not lead to a result where each trajectory took its own unique path, but rather they traveled closely clustered together. This degenerate grouping was due to all start locations being in such close proximity relative to the size of the meteorological grid used. The North American Mesoscale (NAM) Forecast System meteorological data was used, having a horizontal resolution of 12 km, which is larger than the trajectory start area. An ensemble of 27 particles was started every three hours centered at the emission site 100 m and 500 m above ground-level. The sensitivity to the start height was determined to be minimal by comparing trajectory ensembles over the 59 runs performed from August 9-15. In HYSPLIT, an “ensemble” starts all trajectories in

the same location, which is sufficient for a small emission area as in the Nova Scotia fire, but uses meteorological data that has been shifted by one grid box in the horizontal and 0.01 sigma units in the vertical, creating 27 ensemble trajectories that diverge according to the meteorological vectors driving them. The particle's transport was modeled for 24 hours and a plot was created to visually display the path of the particles every hour throughout the wildfire burn duration and during the time for which infrared spectra were collected at the TRSL.

The Alberta wildfire is 1000 times larger by area, so a matrix of 27 trajectory start points was used to fill the area of emission. These trajectories were started every 24 hrs at 500 m above ground-level. Global Data Assimilation System (GDAS) meteorological data, with a resolution of one degree in latitude and longitude (approximately 100 km by 60 km in Fort McMurray), was used and the particles were modeled for 168 hours (7 days), to account for the much greater transport distance.

Transport modeling for the Seven Mile Lake wildfire indicated several times of potential air mass transport from the wildfire emission site to Halifax. Table 5 shows a summary of these results where three timeframes were identified as having some level of direct transport to Halifax near continuously throughout each time frame. The likelihood of transport was defined by the number of trajectories, as a percent of the total, within a box (shown in yellow in Figure 24) around Halifax that is either the size of one or four meteorological grid boxes. Weak likelihood of transport is defined as at least three trajectories, 10 percent of the total, passing within 24 km of Halifax, moderate likelihood is defined as at least three trajectories passing within 12 km, and strong likelihood is

defined as at least six trajectories within 12 km. The likely transport arrival times from the Seven Mile Lake wildfire to Halifax can be interpreted as three temporal regions during which various strengths of transport were occurring (Full list of transport found in Appendix B: HYSPLIT Trajectories).

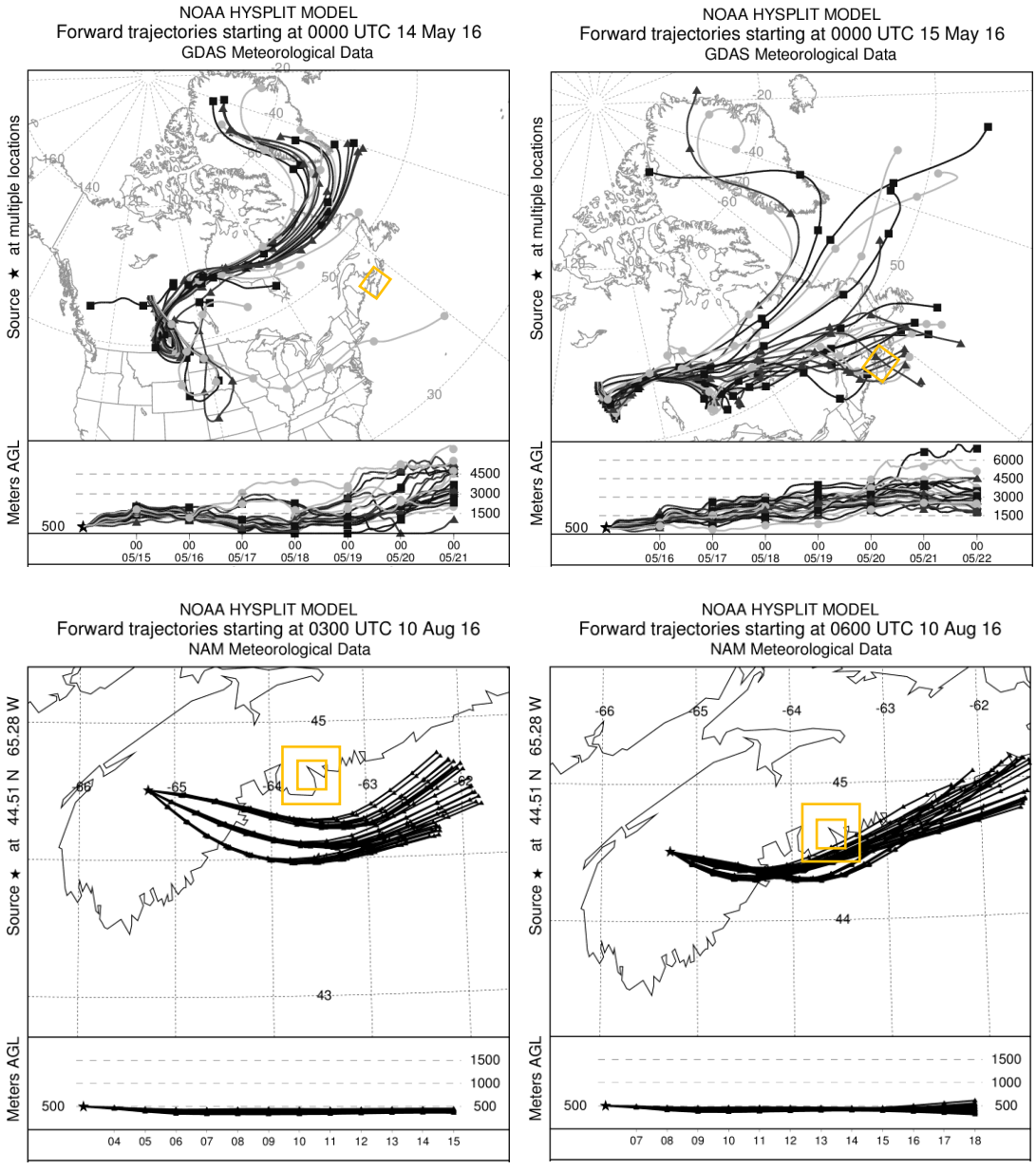

Figure 24: Sample HYSPLIT trajectory maps for air masses from the Fort McMurray and Seven Mile Lake events. Yellow squares represent the boxes around Halifax used to identify if transport occurs or not.

Table 4: Nova Scotia wildfire "likely transport" arrival times based on 24 hour trajectory calculations initiated every 3 hours for the wildfire duration. Full detailed table in Appendix B: HYSPLIT Trajectories.

Summary of Transport Arrival Times in Halifax	
From	**To**
August 10 13:00	August 10 15:00
August 11 17:00	August 13 01:00
August 14 20:00	August 15 01:00

Transport modeling for the Fort McMurray, AB fire shows much more dispersion of emissions, as expected. There are few days when the emissions can be deemed as likely to be moving towards Nova Scotia. Trajectory maps were checked for instances where trajectories passed within a 200 km by 200 km grid around Halifax and vertically under 1.5 km. This region was chosen horizontally based on the size of a meteorological grid box in the GDAS data used and vertically based on an approximate height of the planetary boundary layer, which dictates ground-level mixing with the mid-troposphere. Trajectories that passed within horizontal proximity to Halifax, such as on May 15 (Figure 24), comprised of 15 of the total 61 days (May 1 – July 4) that trajectory runs were performed. The particles that did pass within that horizontal grid box were at altitudes between 1.5 km and 6 km, with one exception of a single trajectory passing through at a height of 700 m on May 16.

An aircraft campaign by NASA called the North Atlantic Aerosols and Marine Ecosystems Study (NAAMES) included a High Spectral Resolution Lidar mounted to the bottom of the aircraft, which was used to observe vertical profiles of aerosols and clouds. One NAAMES flight passed over Sable Island, NS on May 13 (coincident with the Fort McMurray, AB wildfire duration) and observed elevated aerosol levels in the mid-troposphere (Figure

25). The group utilized HYSPLIT and fire count data and concluded that the observed aerosol plume was transported from the Fort McMurray fire (Denise Lineberry, 2016). This airborne LIDAR data helps validate the HYSPLIT trajectories calculated in this study and the overall approach of using air mass parcel transport as a proxy for emitted trace gases.

From the HYSPLIT trajectories and the NAAMES aerosol profiles, the majority of any emission transport from Fort McMurray, AB to the east coast arrive at an altitude between 1.5 km and 6 km and widely dispersed over a large area. Detectability at ground-level is unlikely given these results, which is not unexpected for transport on a continental scale.

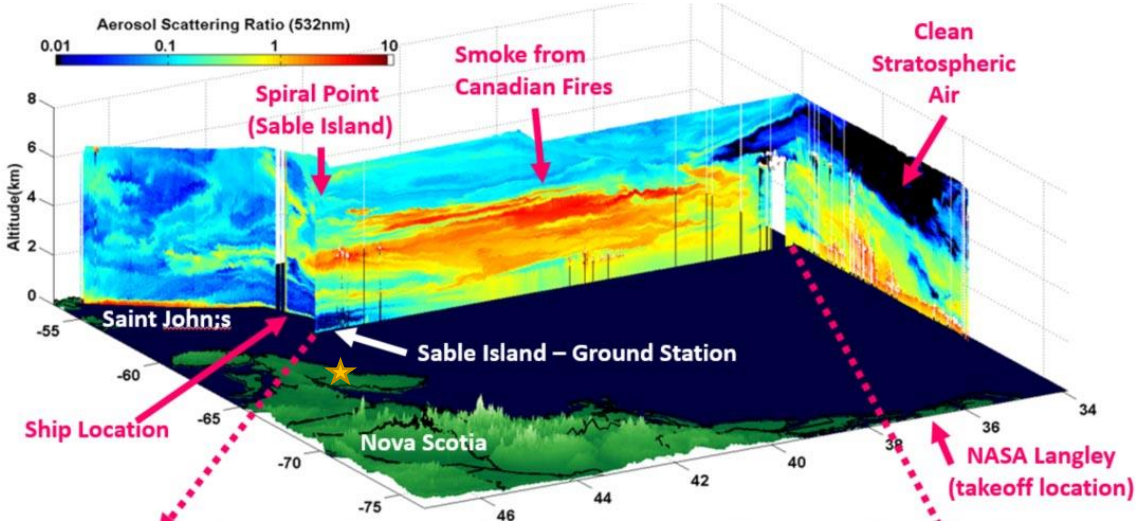

Figure 25: NAAMES vertical aerosol profile on May 13th where the star marks the location of Halifax (Denise Lineberry, 2016).

3.3. Retrieval Method

Retrievals were performed on OP-FTIR spectra from the two biomass burning event campaigns. All trace gases listed in Table 3 were retrieved, with varying levels of success.

The majority of the gases had been previously retrieved by Dr. Li Li, so the retrieval parameters were already sufficiently optimized. However, retrieval parameters were researched and tested for acetic acid (CH3COOH) and hydrogen cyanide (HCN) in this work because they had not previously been retrieved by our lab.

The Open Path System has a retrieval algorithm built into its acquisition software, called OPUS_RS. This software is used for getting real-time retrievals in the field during the measurement process. For in-depth research of various field case studies, the retrievals are again performed using the MALT software (Griffith, 1996), which affords several advantages, described below.

MALT performs retrievals using a non-linear least squares (NLLS) iterative fitting routine that matches measured and forward modeled spectra (Griffith, 2012). The NLLS fitting routine accounts for non-linearity of Beer's law in cases of moderate to strong absorption, when concentration is no longer directly proportional to absorbance. Instead of fitting absorbance, transmittance spectra are fit to minimize a least squares cost function based on a difference or "residual" between the calculated and measured spectrum. If the residual is high or shows systematic features, it indicates that a particular feature or number of features are not being correctly fit by MALT. To calculate or "forward model" a spectrum to fit to a measured spectrum, the program uses input information on the instrumental lineshape parameters, atmospheric conditions, and reference spectral absorption coefficients of all target and interfering gases. The instrumental lineshape describes the lineshape produced from the instrument response to a perfect monochromatic source. An example fit is shown in Figure 26, where the fit is good (low

residual) through most of the micro-window but shows some residual feature <5% around 2075 cm^{-1} not being fit as well as the rest of the spectral window. The fit includes H_2O and CO as interfering gases, but the main target of the retrieval is to find a CO_2 concentration that gives the best fit.

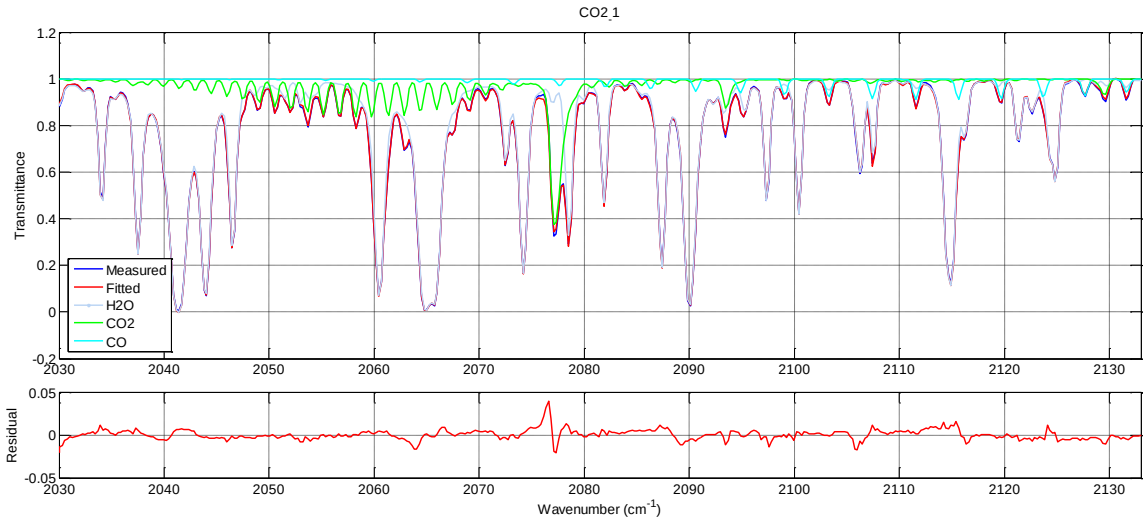

Figure 26: Example fit for CO_2.

Spectral absorption is both temperature and pressure dependent, so these variables are recorded using a Davis Vantage Pro 2 weather station and used as inputs for MALT. The software inputs the spectral position and intensity of absorptions for each molecule from a database of either measured or calculated reference spectra. One reference set is the HITRAN 2012 database consisting of individual line absorption coefficients for 47 common and small molecules (Rothman et al., 2013). When HITRAN is being used, reference spectra are calculated line-by-line from the absorption coefficients, pressure, temperature, an initial guess for the absorber amount, and knowledge of the absorbing path length. Instrumental effects are also convolved with the theoretical or true lineshape

to accurately model the measured lineshapes. The other reference set is the PNNL database which was created by measuring the individual spectra of pure samples of nearly 500 species (Sharpe et al., 2004).

The PNNL spectra are measured at a resolution of 0.1 cm^{-1}, which is degraded to match our lower (0.5 cm^{-1}) resolution. One major advantage of MALT over the native OPUS_RS software, which uses PNNL reference spectra, is that PNNL spectra are recorded at only two or three temperatures (50 ^{o}C, 25 ^{o}C, and sometimes 5 ^{o}C), while HITRAN-calculated spectra are calculated at the precise path-average temperature supplied to the retrieval. This eliminates errors associated with OPUS_RS interpolating reference spectra between, e.g. 25 ^{o}C and either 50 ^{o}C (in summer) or 5 ^{o}C (in winter), and assuming the 5 ^{o}C spectrum exists (Sharpe et al., 2004).

One advantage of OPUS_RS over MALT, besides the real-time retrievals, is in the case of complicated (i.e. non-polynomial) spectral continuum shapes, which can be fitted more accurately with the Gaussian functions available in the software algorithm.

Various parameters that describe the measurement conditions (e.g. absorption path length) and influence the instrument line shape (e.g. resolution) are set at a specific value and either remain fixed or they are fit by MALT. Commonly used and modified parameters are summarized in Table 5. Fixing, versus fitting, well known parameters (e.g. resolution, path) or choosing to fit more variable parameters (e.g. wavenumber shift) can improve the fit of the spectra.

Table 5: Spectral fitting parameters within MALT software (Griffith, 2012; 2016).

Parameter	Description	Fix or Fit	Typ. Value
Pressure	Atmospheric pressure, path-averaged, at time and place of measurement	Fixed	1013.25 mbar
Temperature	Atmospheric temperature, path averaged, at time and place of measurement	Fixed	25 ºC
Pathlength	Two- way distance IR light traveled	Fixed	500 m
MALT components	Number of HITRAN gases for which absorption coefficients are to be calculated in a single retrieval	Fixed	1, 2, 3…
Library components	Number of PNNL reference spectra to use in a single retrieval	Fixed	1, 2, 3…
Polynomial	Terms in polynomial fit to spectrum to account for broad continuum absorption due to the window, beamsplitters, mirrors, detector response, IR source strength	Fit	1 = constant 2 = slope + intercept …
Shift	Spectral shift in wavenumbers, which depends on stability in interferogram sampling	Fit	0.0
Resolution	Spectral resolution, taken as 1/(max OPD), affects linewidth and lineshape	Fixed	0.555 cm^{-1}
Apodisation	Apodisation function, affects lineshape	Fixed	Triangular
FOV	Field of view of the spectrometer in mrads, affects lineshape, theoretical = apodisation/focal length = (3/69)	Fixed	20 mrad
FAP	Effective apodisation, accounts for symmetric instrument line broadening due to imperfect beam collimation	Fit	0.0
Phase	Phase error, corrects asymmetry in instrument lineshape caused by errors in zero path distance	Fit	0.0 ^{o}
SYM1, SYM2	Asymmetry functions, accounts for badly aligned spectrometer, helps fit asymmetric lineshapes	Fixed	0.0

MALT outputs a variety of information along with the fitted spectra and retrieved concentrations that can be used to determine the quality of the retrieval. A list of the percent error for each gas fit is a good place to start. If a retrieval results in a large error, a correlation matrix of the fitted parameters and fitted concentrations can indicate if any

fitted component is dependent on another one. For example, the retrieved (or fitted) trace gas concentration can show a high correlation with another trace gas, if they are highly overlapped in the spectrum, pointing to a source of error that may be mitigated. The residual or spectral “misfit” is calculated from the difference between the measured and fitted spectrum in the retrieved spectral window and can indicate where in the window the largest errors are occurring, helping to identify which spectral feature is not being fit optimally. In the case of high residual, the number of iterations MALT performed for the fit may indicate that there is difficulty converging to a fit of a feature in the spectrum.

MALT is used for performing retrievals on single spectra, however there is no comprehensive built-in function for performing retrievals on large datasets. Typically a spectrum is taken every minute, leading to over ten thousand retrievals for a week’s worth of data. To facilitate the large data processing load, Dr. Li Li created MATLAB scripts to perform batch retrievals on the data and its visualization, which were streamlined, repackaged, and documented in the course of this project. The repackaging is a set of MATLAB files with instructions and an explanation of the program flow, Figure 27.

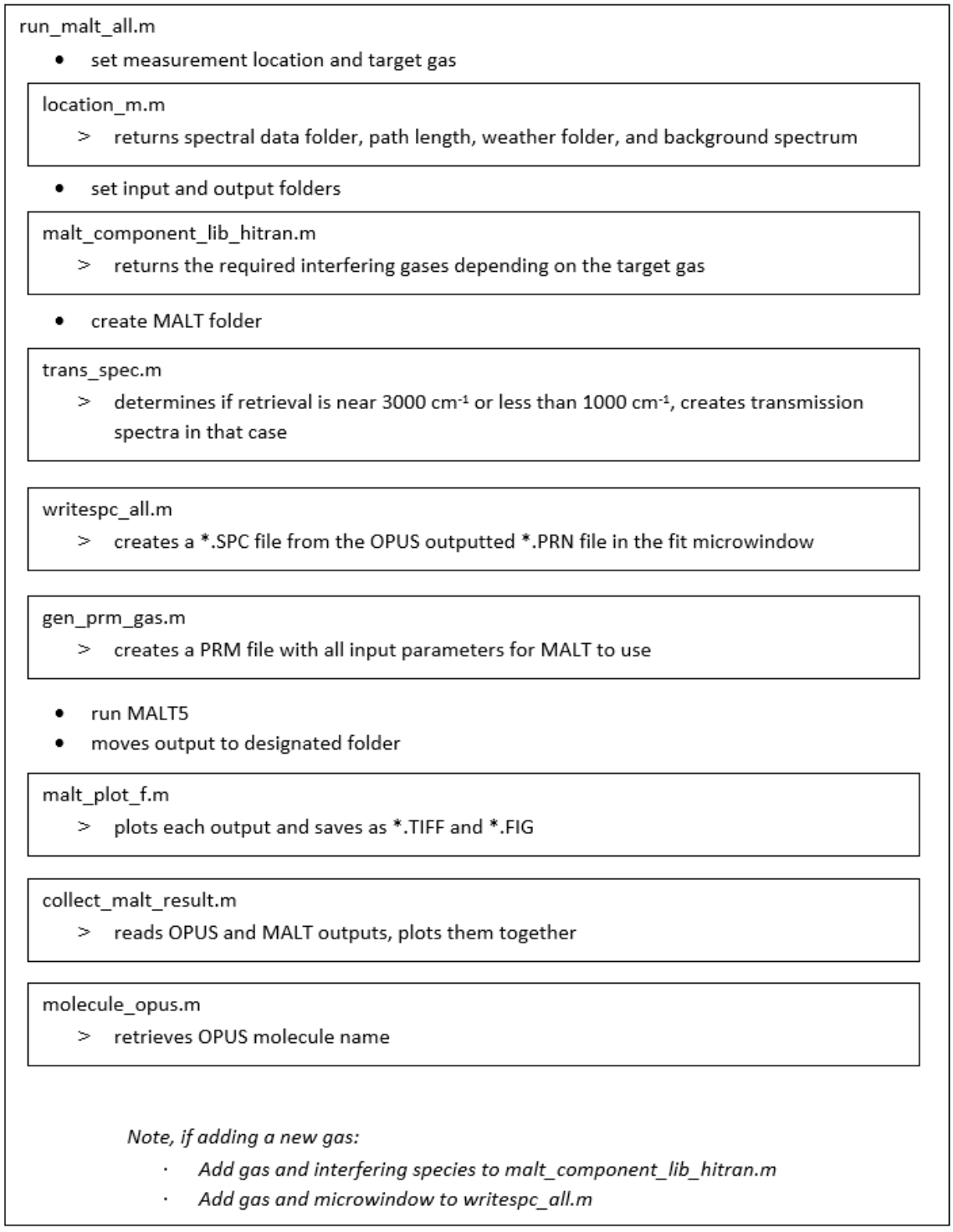

Figure 27: Schematic of MATLAB scripts to process large data sets of OP-FTIR observations. Each box represents a MATLAB script.

In the biomass burning study, initial parameters were determined by looking at reference spectra for the spectral positions of absorptions of target gases and any potential interfering gases. Other reported studies of wildfire emissions using OP-FTIR were also consulted when determining retrieval parameters of CH_3COOH and HCN (Smith et al., 2014). Example fits for each retrieved gas are shown in Figure 28. The plots typically show residuals as low as 0.1% (e.g. methanol (CH_3OH)) and as high as 5% (e.g. CO_2), indicating generally good fits for all trace gases. In the case of HCN retrievals, a section of the microwindow between 720-725 cm^{-1} was not being correctly fit (Figure 28), noted by the residual nearly reaching a magnitude larger (10%) than the rest of the fit (1%). To correct this, additional interfering gases were looked for, parameters were checked for errors, and ultimately there was no improvement, likely because errors stem from imprecise spectral parameters. The solution to this problem was to de-weight the spectral region with higher residual values from 720-725 cm^{-1} so that the misfit in that region was not influencing the iterative scheme working to minimize the difference between the measured and modeled spectrum, and ultimately the final retrieved gas concentration values. The low residuals in Figure 28 are a result of carefully choosing the microwindow in which the target gas absorbs strongly but is not heavily interfered with by other gases, especially water vapour. All unavoidable interferers must be accounted for if their absorption is above noise levels. When performing fits, any large spikes or structured features (not white noise) in the residuals need to be analysed and minimized. The ability to retrieve a trace gas partially relies on the absorption of the target gas being larger than the level of noise, e.g. the low absorption of CH_3OH compared to even lower noise.

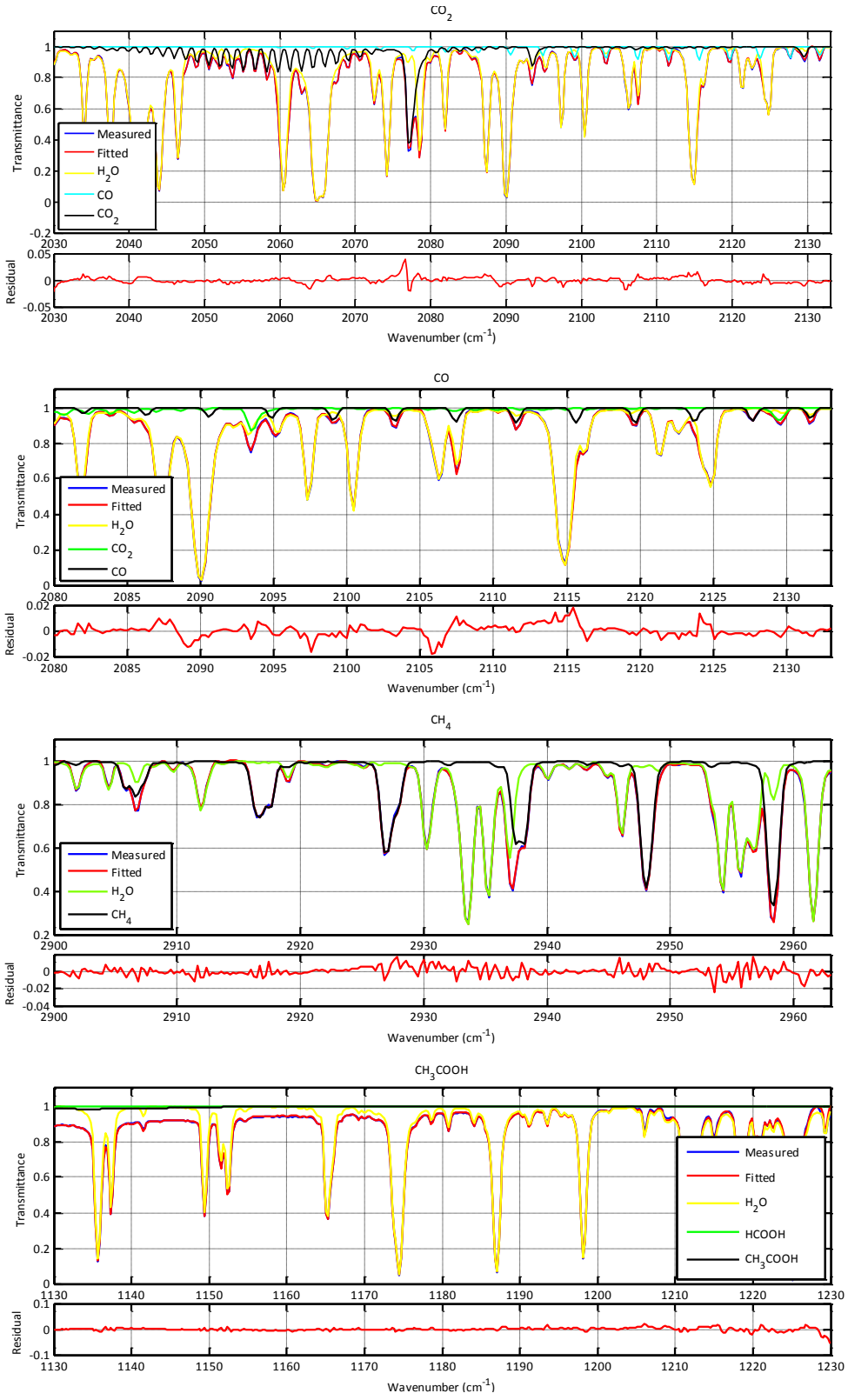

Figure 28: Example fit from August 9, 2016 at 12:25 of each retrieved biomass burning tracer identified in Table 3.

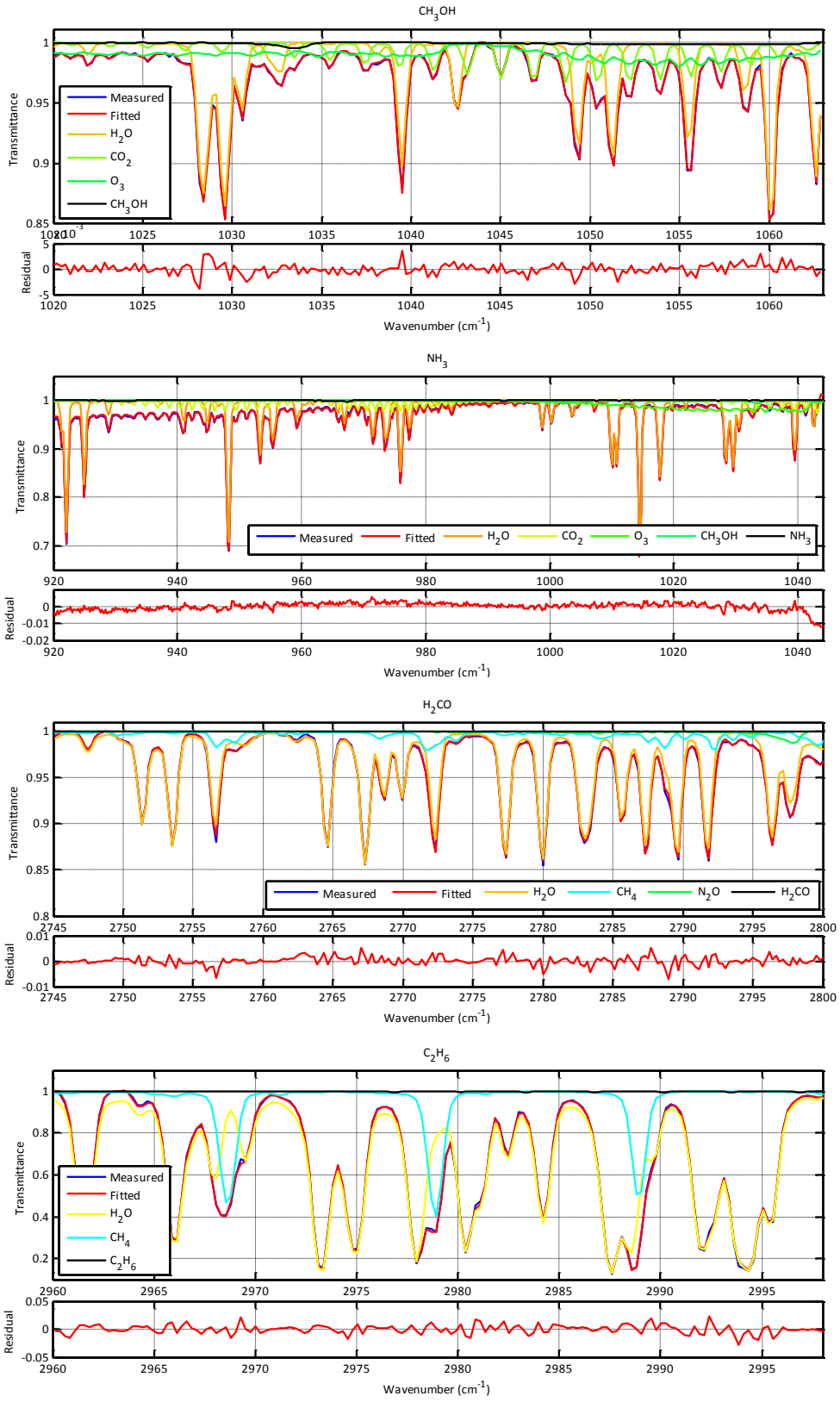

Figure 28 Continued: Example fit from August 9, 2016 at 12:25 of each retrieved biomass burning tracer identified in Table 3.

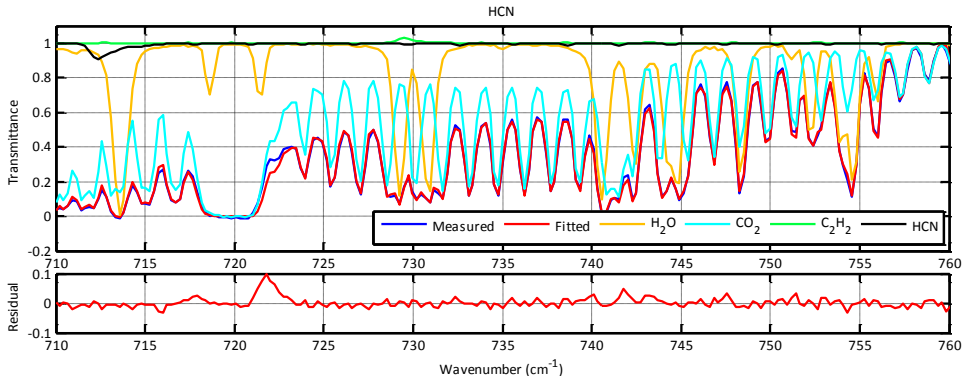

Figure 28 Continued: Example fit from August 9, 2016 at 12:25 of each retrieved biomass burning tracer identified in Table 3.

Beyond looking at spectral fit residuals, optimizing the fit of a spectrum involves also analysing other output information from MALT such as the "housekeeping" file. The housekeeping file (*.hkp) shown in Figure 29, recaps for each individual retrieval information on the instrumental fitting parameters (lines 9-21), the atmospheric path and spectroscopic input information used (lines 23-31), and, crucially, the correlation matrix between fit parameters (lines 34-44), as well as the retrieved values (with errors) for the target and interfering gases and fitted instrumental parameters (lines 46-58). This housekeeping file can point to correlations between retrieved parameters experiencing "cross-talk". The correlation matrix shows if any parameters are being influenced by the fit of any other parameters. The retrieval result and error can be used to show some confidence that a particular parameter was fit well. In the example file in Figure 29, CH_3COOH has a high percent error and a high correlation with retrieved shift and phase parameters. The solution to correct any irregularities is to try setting and/or modifying one of the parameters and retrieving again.

Some data in the time series, to be presented next, have been removed due to an insufficient infrared signal through the path, due to heavy fog and/or rain. The cut-off infrared signal was determined by examining the root mean squared (RMS) of the fit to measured residual across the retrieval microwindow for each gas versus the infrared signal (Figure 30). A cut-off of 0.1 was chosen for the time series because the RMS of the residual in individual fits does not degrade until the infrared signal drops below that level for the gases considered. The RMS of the residual is a useful diagnostic of overall noise in the spectra and large mis-fitting issues, but, as a single number, it does not give details of the quality of spectral fits of particular absorption lines in the retrial window under consideration.

```
MALT5.5.9 151202                  Run 08/02/2018  18:57

Fitfile
C:\FTIR_data\2016_08_09_Rice_NSfire\(2016_08_09_12_25_51)_Measurement\MALT_2016\Acetic\SPC\Acetic_1.spc
Input                         malt_para.prm
Comment                       Remote
Output                        c:\malt5\fts\output_file.*
Bgndfile

Output region +/- extension    1129.661       1229.947          9.884
Full calculation region        1118.090       1241.519
Grid (high, low)               0.007533       0.241072
Npts (high, low, out)             16384            512            417
Apodisation, fit resolution    NB77-med          0.556
Init_shift, SNR                   0.000             0.
FOV, eff. apod.                  20.000          0.000
phase, misalignment               0.000          0.000
sym1, sym2                        0.000          0.000
pressure shift, FOVshift              T              F
Voigt vary, width, cutoff           0.0          200.0        0.0E+00
FOV by FT                             T
Grid per atm                      0.010

Layer 1: Sample
P/mb, T/K, path/m              1018.500   295.760   685.700
broad, isoscale                   0.000         0
Mol   Iso       vmr    #lines    alfaL     alfaD
Linelist                              sec
H2O     0  1.00E-02      1137  0.061000  0.002055
c:\malt5\hitran\H2O.mir             0.11
HCOOH   0  1.00E-09     12539  0.101585  0.001286
c:\malt5\hitran\HCOOH.mir           0.42

Library spectra                    amount
C:\Malt5\PNNL_lib\AceticAnhy_25T.spc       1.0000 ppb


Correlation matrix
==================
             H2O      HCOOH    Acetic   poly1    poly2    shift    fap
             phase
      H2O   1.0000
    HCOOH   0.0459   1.0000
   Acetic  -0.1276  -0.6663   1.0000
    poly1   0.4231  -0.1455   0.5417   1.0000
    poly2   0.2553   0.0105  -0.5238  -0.3329   1.0000
    shift   0.0129   0.1347  -0.1819  -0.1248   0.3372   1.0000
      fap   0.4624   0.0294  -0.0856   0.2718   0.1653   0.0186   1.0000
    phase  -0.0102  -0.1867   0.2492   0.1730  -0.4512  -0.7567  -0.0217   1.0000

Fitted parameters for
C:\FTIR_data\2016_08_09_Rice_NSfire\(2016_08_09_12_25_51)_Measurement\MALT_2016\Acetic\SPC\Acetic_1.spc
=================
   Parameter      value              error     %error
   H2O           1.0234  %         0.004320     0.422%
   HCOOH         9.4133  ppb       5.561312    59.079%
   Acetic        3.8415  ppb       0.534480    13.913%
   poly1         0.9770            0.000668     0.068%
   poly2         0.1521            0.002811     1.849%
   shift       -0.00660  cm-1      0.001429    21.646%
   fap          0.14158            0.011675     8.247%
   phase       -0.43216  deg       0.136437    31.571%
   resid     0.00689407
   iterations         6
```

Individual Retrieval File Housekeeping Info

Instrumental and Computational Parameters

Atmospheric Path and Spectroscopic Inputs

Correlations Between Retrieval Parameters

Retrieval Results, RMS of the Residual, and Iterations

Figure 29: Housekeeping file for CH_3COOH retrieval.

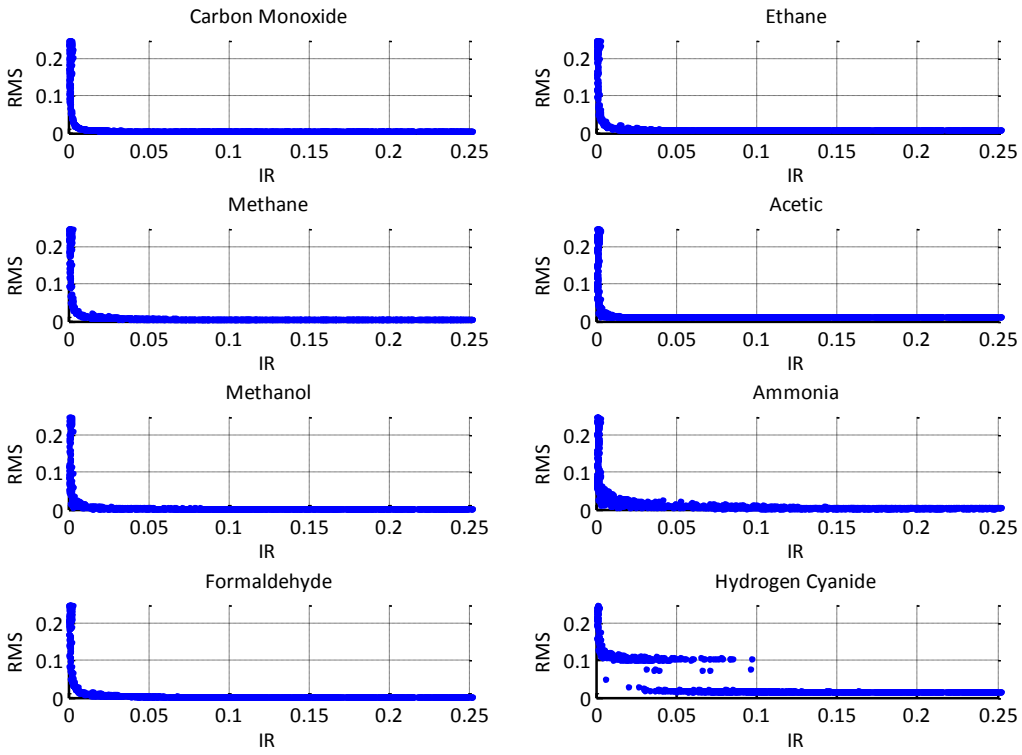

Figure 30: RMS of the residual (0.1 = 10%) versus infrared signal for target trace gases for a series of individual retrievals shown in Figure 32.

The time series of water (retrieved with CH_4) and the biomass burning tracer gases from Table 3 are shown in Figure 32, while the corresponding environmental parameters recorded during the measurement period are included in Figure 33. These datasets were examined for features that could indicate a detection of biomass burning during and near likely times of biomass burning emission transport.

Starting with CO, there was one large enhancement to >350 ppb that lasted a few hours between 08:00 – 11:00 on August 10. Possible local sources of the large concentration enhancements were examined, one being ships in the nearby harbour. Figure 31, created

by Dr. Li Li, shows ship locations for the peak of the morning enhancement. The locations of ships and the wind direction indicate that ships were not the source of the enhancement. Additionally, it is not likely from other industrial sources because the wind was not from the Halifax core or surrounding industrial areas to the North of the measurement location. The other activity in CO is enhancements in the evening of August 9 to 12, is possibly a result of weekday evening rush hour traffic. The days where this evening enhancement occurs experienced winds from the north (toward city core) around the same time as the enhancements.

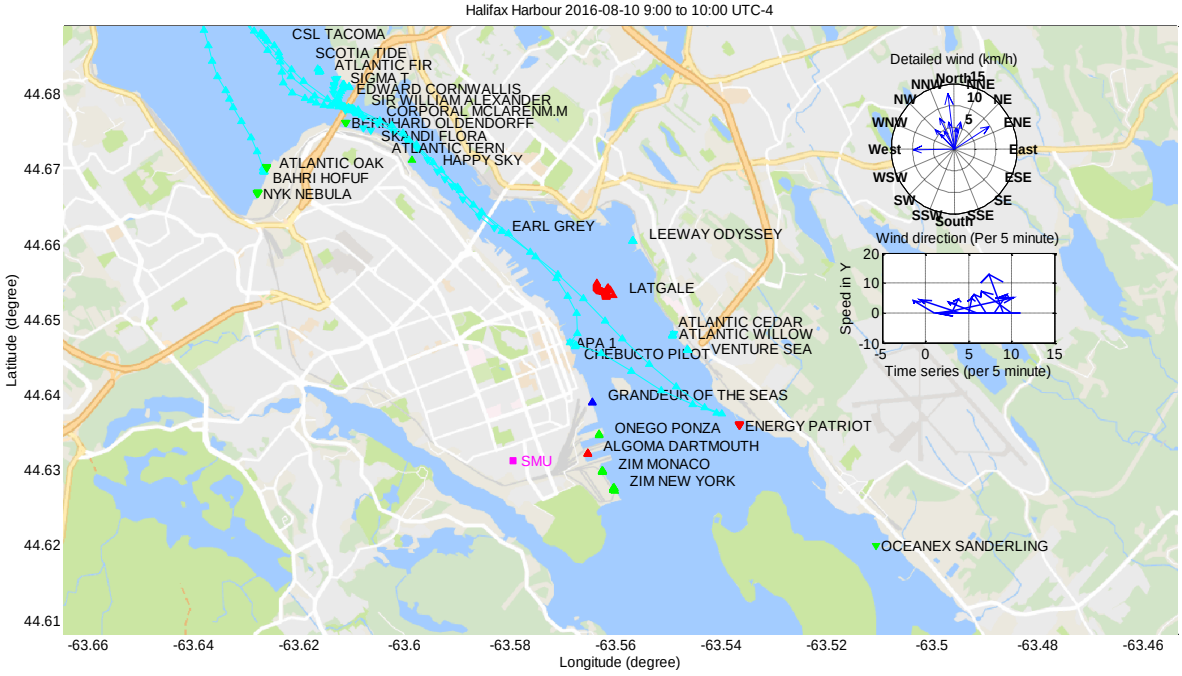

Figure 31: Plot of shipping locations and routes during peak of CO event on August 10 from 09:00 – 10:00.

For CO_2, distinct enhancements can be seen August 10 and 12 mornings around rush hour. There is also some increase in CO_2 around midnight August 11, and more prominently

August 13. The largest enhancements tend to occur after periods of low wind speed (Figure 33) such as less than 10 m/s on August 10 morning, August 11 afternoon, August 12 and 13 evening, likely a consequence of local emissions having the opportunity to "build up" during these times when the transport is minimal and the accumulation is high.

CH_4 shows an interesting pattern of increasing around midnight every other night. The bi-nightly increase could possibly come from a similar pattern in wind speed, where slow wind speed nights correspond to enhancements in CH_4. This could be due to a local emission source that is only active during some nights, or only has the opportunity to build up in the atmosphere when the wind is low enough that transport is minimal, or a combination of these factors. Longer time series will help clarify the nature and frequency of such events.

CH_3COOH has a sharp (>8 ppb) enhancement that lasts for only one minute at 09:50 h on August 10. The short duration of this spike indicates that it is likely from a very local source and has not had the time to disperse. Additionally, the instrument's sensitivity to wind direction when it comes to isolated local sources may be a factor in this spike. Since the path of detection is long (a few hundred meters) and narrow (thirty centimeters) then sources that are emitted and transported along the path are in the detectable path a larger portion of the one minute co-adds compared to those transported perpendicular to the path length. The other noticeable feature for CH_3COOH is that it tends to correlate weakly with water concentration at times (more on correlation between gases below). Correlation between CH_3COOH concentrations and water in the retrievals should be explored in future work.

CH_3OH has one outlying feature at 19:00 on August 10 that lasted for five minutes and peaked at 74 ppb (15x baseline values). Note that the plot in Figure 32 is limited in the concentration axis as to display other features outside of this spike better. This is likely a local source and also occurred during a time when the wind direction was along the path of detection, potentially related to the sampling bias discussed in the single CH_3COOH spike, though during a different time. The retrievals during the spike were also assessed individually, due to the short spike's irregularity in the time series, to rule out a problem with them (e.g. large errors) but they did not show any anomalies (i.e. RMS of the residual, spectral residual, and percent error similar to neighboring points in time).

NH_3 has some minor enhancements during the nights of August 9 and 11 and one larger enhancement near midnight on August 12 well above the 1.1 ppb NH_3 detection limit provided by Bruker for a shorter path. The formaldehyde (H_2CO), ethane (C_2H_6), and HCN retrievals are also noisy due to their low concentrations (detection limit 2 ppb) and show the concentration sometimes going below zero, especially for H_2CO. The enhancements that stand out above zero for H_2CO can still be taken as an actual increase in concentration because the retrieval becomes more accurate for higher concentrations of the target gas. However, the HCN retrieval in particular is problematic because the data shows noise in the time series at 10 ppb levels around a typical value of ~20 ppb while an expected ambient HCN level is 1 ppb. The retrieved levels are higher than the Bruker calculated detection limit from Table 1 of 3.6 ppb, but it is unlikely that the levels of HCN are in fact 20 times a typical ambient level. The retrieval "housekeeping" file shows error in the HCN retrieval up to 40% for the target gas, and up to 140% for the interfering gas C_2H_2.

Additionally, there is a moderate correlation between HCN and CO_2. The low concentrations of HCN in the atmosphere make it difficult to perform accurate retrievals and these should be looked at in depth in the future. For example, retrieved interfering C_2H_2 values were negative, which points to a systematic and unphysical retrieval issue with crosstalk between HCN and C_2H_2 in the HCN window. C_2H_6 retrievals on the other hand do not appear strongly impacted by reduced IR signal levels (Figure 33), while the opposite is the case with retrievals of NH_3, H_2CO, and HCN, which tend strongly to negative values in these instances. This is another systematic feature to investigate in more detail in the future.

One enhancement is visible during the morning of August 10 between 08:00 – 11:00 for both H_2CO and C_2H_6 (and possibly HCN). This morning enhancement aligns with a strong increase in CO (>350 ppb), and some weak increase in CH_4, CH_3COOH, and CH_3OH as well. The HYSPLIT trajectory calculations indicate that transport was likely to arrive between 13:00 – 15:00 on Monday. The proximity in time of this enhancement and the likely transport arrival is a possible indicator that the enhancement is from biomass burning emission transport from the Seven Mile Lake wildfire to Halifax, even though the time periods are separated by two hours. No comparable trace gas signatures (in terms of CO) are present in time series on August 12 - 13 and August 14 - 15, which were the other times of likely transport from the NS wildfire to Halifax, according to trajectory modelling (Table 4). It is worth noting here that in previous campaign-based measurements carried out by the laboratory in 2015, CO did not exceed 250 ppb during a time of high ship activity and favourable transport from the harbour on one occasion (August, 2015), and

also during a very busy vehicular traffic emissions morning on the Tuesday after Labour Day in 2015 (Purcell, 2016). Again, with longer observation time series such as will be possible with the TRSL, patterns between concentrations and emissions sources will become clearer.

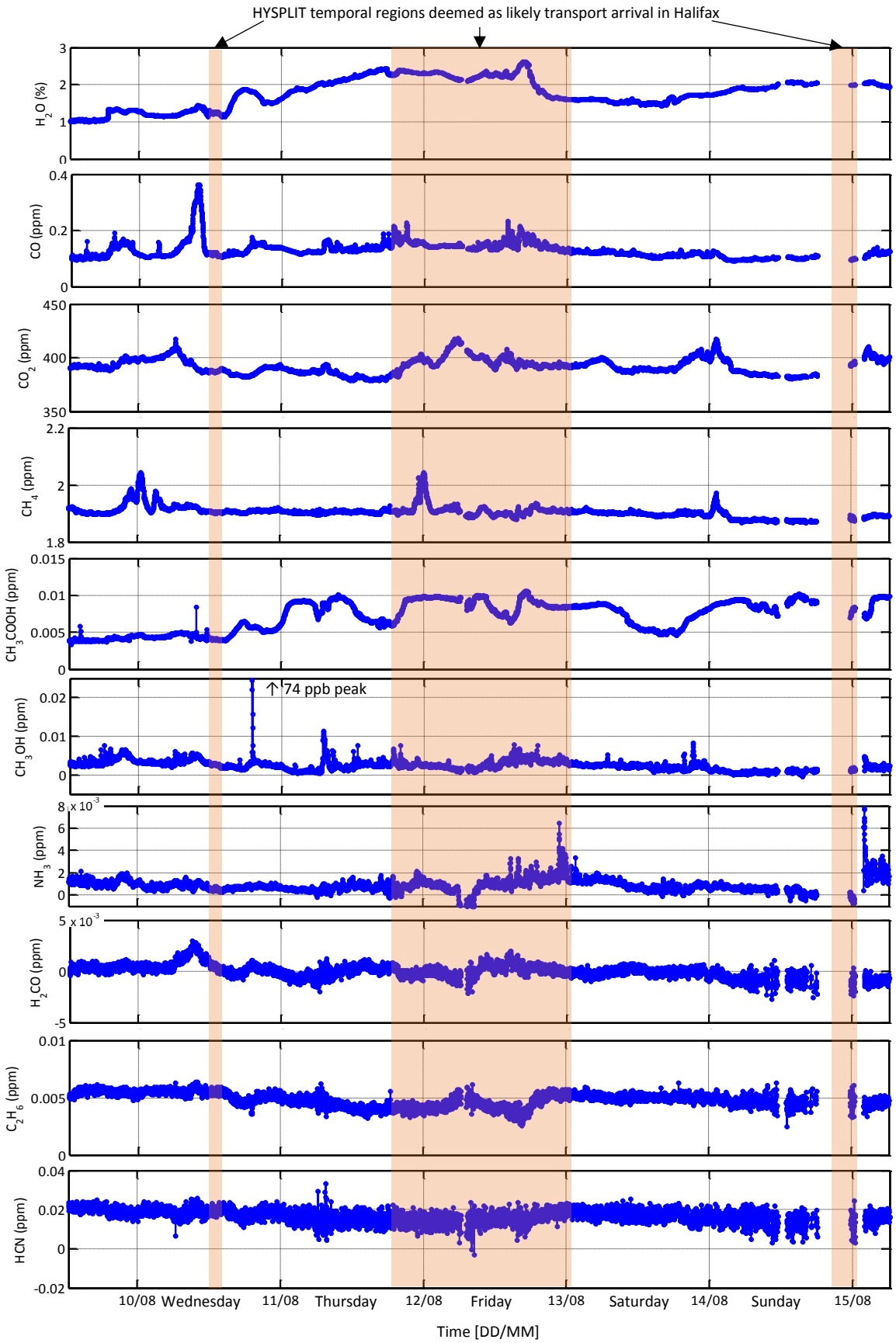

Figure 32: Full time series of retrieval results from Seven Mile Lake wildfire campaign in 2016.

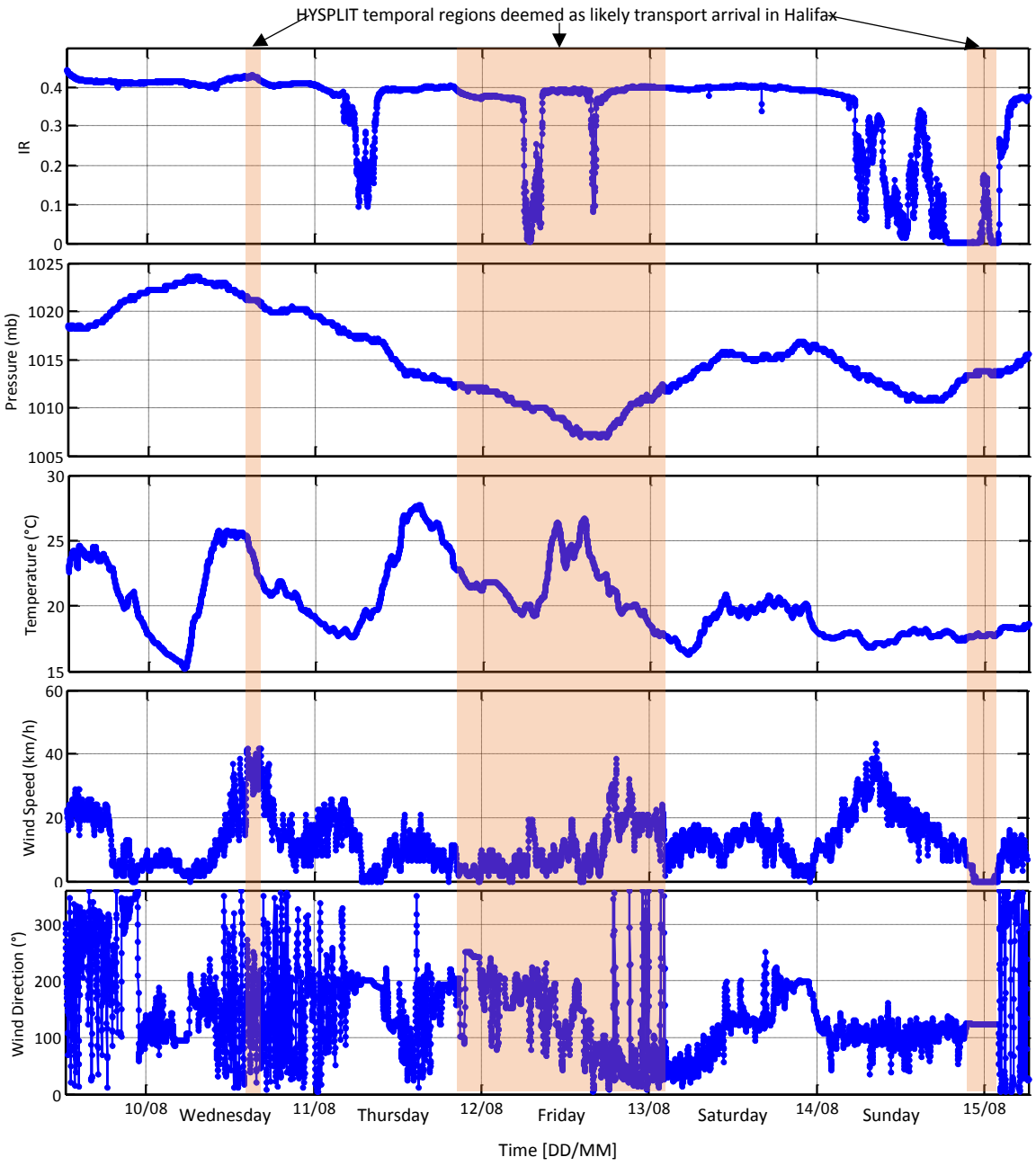

Figure 33: Environmental parameters during Seven Mile Lake wildfire event in 2016.

A useful tool for emission studies is to examine the correlations between different gases in time. The reason is that while there are several potential emission sources for each of the gases in this study, emissions from biomass burning will be high in several of these gases simultaneously. If multiple gases are enhanced at the same time it is a stronger

indication that the emissions are from a biomass burning source versus another potential source (Smith et al., 2014). Figure 34 shows the correlation of the various trace gases retrieved in this study. CO is used as the gas to compare to because it is heavily emitted from biomass burning incomplete combustion (Table 3) and is retrieved well from OP-FTIR spectra. The correlation plots can expose times when individual gases increase simultaneously with CO or alone more clearly than in a time series analysis. In the cases of CH_4 and NH_3 there are times of enhanced target trace gas independent of CO, indicating a non-combustion source. There are noticeable correlations between H_2CO, C_2H_6, and HCN with CO during the August 10 CO enhancement, displaying as positive slopes in the plots.

Times deemed likely for transport of biomass burning emissions by the HYSPLIT trajectories, summarized in Table 4, were examined for correlation compared to the overall correlation of the gases during the entire measurement period. Figure 35 shows this for CH_3COOH, where the data during the first region of likely transport is shaded black.

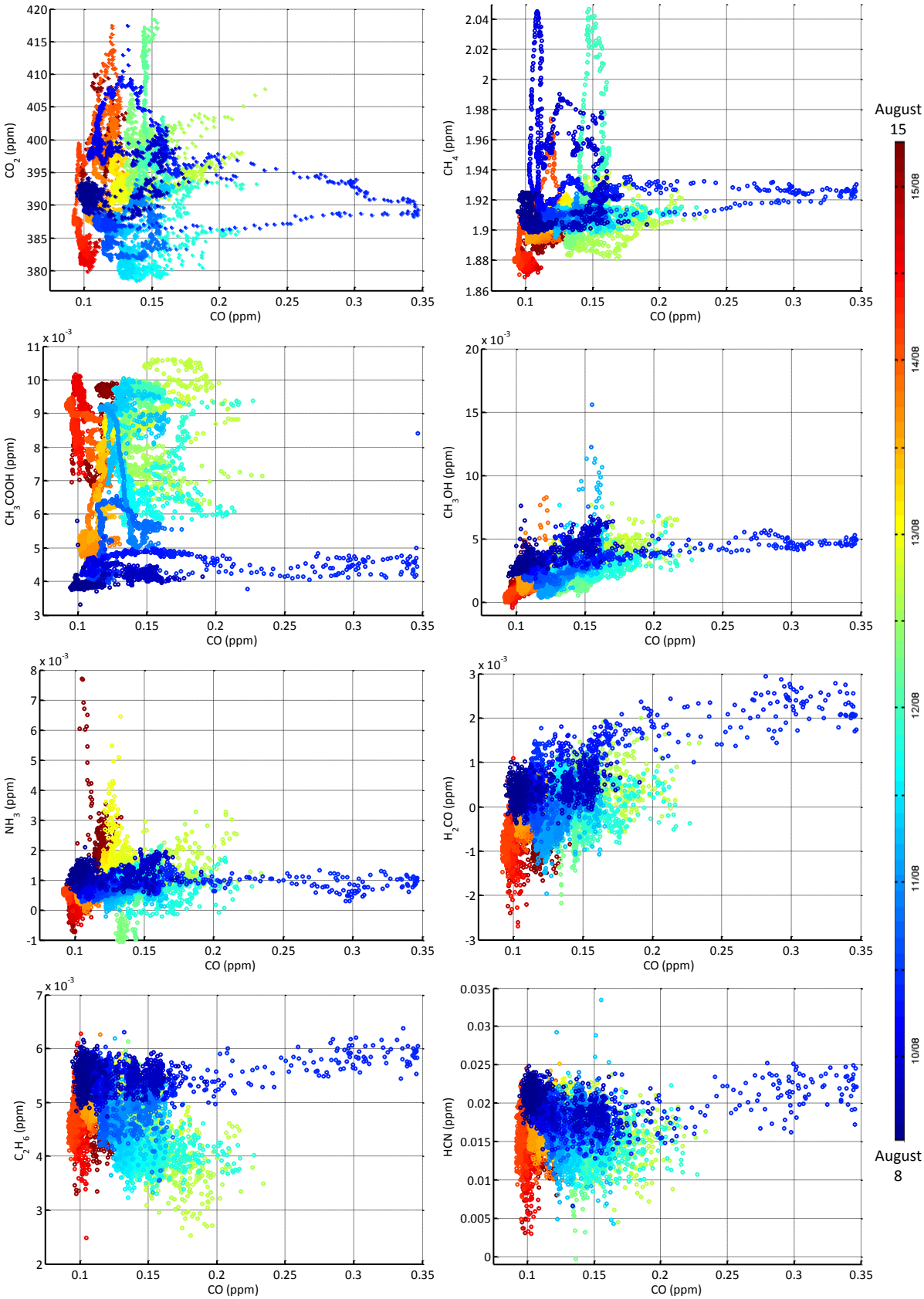

Figure 34: Relationships of trace gases to CO (emission factor decrease for each gas from top to bottom).

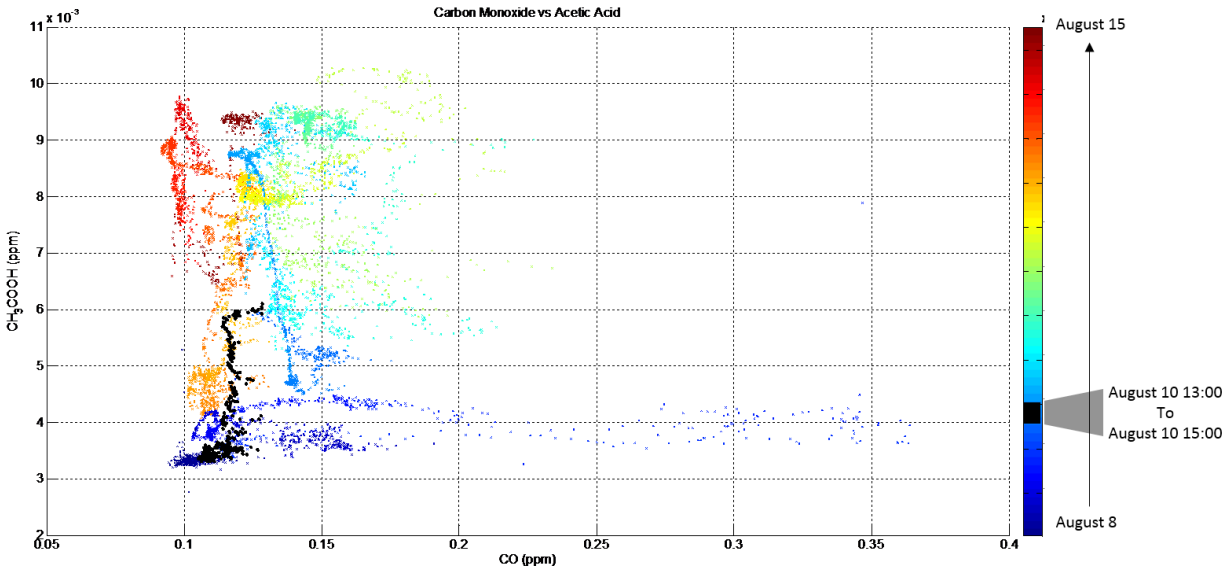

Figure 35: CH_3COOH versus CO during transport time during Seven Mile Lake biomass burning event (August 8 - 15).

The correlation data in the first time interval deemed likely for transport arrival (August 10 13:00 – 15:00), is shown in Table 6. There is a weak correlation between H_2CO and CO but it is negative, not as expected, and no other biomass burning tracers show correlation. This lack of correlation of tracers indicates that the HYSPLIT predicted transport time is not in fact during a period of a biomass burning plume over Halifax.

Table 6: Correlation of biomass burning tracer gases with CO on August 10th from 13:00 – 15:00 (time of predicted plume transport to Halifax).

Trace Gas		R-value (entire time series)	R-value (13:00 – 15:00)	Correlation (13:00 – 15:00)
Carbon Dioxide	CO_2	0.036	-0.270	None
Methane	CH_4	-0.016	0.172	None
Acetic Acid	CH_3COOH	-0.053	0.085	None
Methanol	CH_3OH	-0.033	-0.132	None
Ammonia	NH_3	0.041	0.144	None
Formaldehyde	H_2CO	-0.018	-0.307	Weak
Ethane	C_2H_6	0.0793	-0.190	None
Hydrogen Cyanide	HCN	0.0352	0.102	None

Examining the correlations for gases during the identified unusual enhancement of CO on August 10 from 08:00 – 11:00 resulted in Table 7. There is moderate to strong correlation between CO and four of the other biomass burning tracer gases, indicating that the enhancement is likely from a biomass burning source. Residents of Halifax reported the smell and haze of smoke on the morning of Wednesday, August 10 as additional evidence that the unusual enhancement was a result of the transport of biomass burning emissions from the wildfire (Halifax Metro, 2016). The correlation and temporal proximity to HYSPLIT predicted transport (3-4 hours) suggests that the observed event in the morning of August 10 was direct transport of biomass burning emissions from the Seven Mile Lake wildfire to Halifax. The time discrepancy may be connected to the way that sea breezes are captured (or not captured) in the NAM wind fields, which should be the subject of a future investigation.

Table 7: Correlation of biomass burning tracer gases with CO on August 10th from 08:00 – 11:00 (time of observed elevated CO in Halifax).

Trace Gas		R-value (entire time series)	R-value (08:00 – 11:00)	Correlation (08:00 – 11:00)
Carbon Dioxide	CO_2	0.036	-0.245	None
Methane	CH_4	-0.016	0.245	None
Acetic Acid	CH_3COOH	-0.053	-0.077	None
Methanol	CH_3OH	-0.033	0.819	Strong
Ammonia	NH_3	0.041	-0.311	Weak
Formaldehyde	H_2CO	-0.018	0.695	Moderate
Ethane	C_2H_6	0.0793	0.758	Strong
Hydrogen Cyanide	HCN	0.0352	0.631	Moderate

3.4. Conclusions on Detectability

The Fort McMurray, AB biomass burning emissions are much more dispersed on account of long travel towards NS and result in arrival at a height that would likely not mix downwards and be detectable at ground-level. Compared to all trajectories modeled, 0.07% passed through the defined area around Halifax. To conclusively state whether AB based biomass burning emissions are detectable in Halifax, NS more time dense trajectory calculations (more than once daily) should be completed and longer OP-FTIR measurements should be taken around an event to provide before, during, and after time series. Past work indicates this is possible (Franklin et al., 2014).

The enhancements of CO, CH_3OH, NH_3, H_2CO, C_2H_6, and HCN along with the noted correlations between several tracer gases and CO during that time show that there is likely detection of biomass burning emissions in Halifax, NS from the Seven Mile Lake, NS wildfire on August 10 from 08:00 – 11:00. The HYSPLIT trajectories predicted a transport event of a similar duration but offset by 3-4 hours into the future. This indicates that HYSPLIT modeling can give an estimate of transport directions and times but should not be solely relied on. In addition, it is not clear how well sea breeze events are being captured in the meteorological data driving the HYSPLIT calculations. This should be investigated further.

Finally, the remainder of the biomass burning event duration did not show strong signatures as evidence for detectability, despite the fire growing from August 7 to 11 and not being extinguished until August 22 (Morgan Oikle, personal communication, December 2016). This speaks to the variability in transported tracer gas signatures.

4. Future Work

This project has in part produced the design of a new atmospheric observatory and an examination in detail of a biomass burning case study of detectability by OP-FTIR.

Future work in the biomass burning study could include the performance of a sensitivity study of the transport modeling and a systematic study of certain retrieval characteristics. In particular, some issues of note that emerged in this detailed analysis include: sea breezes impact on transport, trajectory start height, HCN retrieval and bias to 20 ppb with varying RMS of the residual for low IR, as well as the need for additional diagnostic code that evaluates retrieval error, RMS of the residual, retrieved parameter correlation, and iterations. Correlations between retrieved values of CH_3COOH and H_2O, as well as between HCN and C_2H_2 should be examined closely to further evaluate retrieved parameter cross talk. It may also be possible to further optimize, e.g., the CH_3COOH retrieval window in terms of window width and the effects of interfering gas HCOOH. Additionally, the choice of IR signal cut-off should be optimized so as to minimize negative retrieved concentration values, e.g. for H_2CO while maximizing system up time. Future biomass burning events could be studied using the template established in this thesis, also including time series of O_3, which may yield some insight into the chemical age of transported biomass burning air masses. As time series build up, other emissions' accumulation can be studied across various time scales.

The atmospheric observatory may require automation of the open/close function of the spectrometer windows, similar to that of the retroreflector housing. There are provisions

in place in the code and the USB to GPIO board that will allow the solution choice to be simply plugged into the current design. The Python script used for weather data scraping and decision making could be optimized by someone more familiar with the coding language to provide more stability and efficiency with update loops for displayed text in the GUI and exception handling as they arise. The addition of a start/stop of the automation function should be implemented to allow logging of weather data without changing the retroreflector enclosure state. The script would ideally be expanded in scope to control OPUS_RS start and stop functions, the on and off state of the spectrometer (to conserve hardware life) through IP commands or relay control of power, real time retrievals using MATLAB scripts, and storage of outputs on a server for website access. Additionally, large datasets will require a storage solution be put in place to handle an approximate 20 Gb per week of one minute averaged data or 1 Tb per year for the measured spectra, supporting files, and retrieval results combined.

Appendix A: OP-FTIR Standard Operating Procedure

This page left intentionally blank.

OPS Standard Operating Procedure v1.5

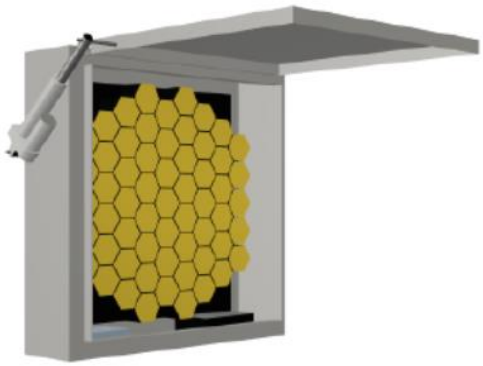

Written by Keane Tobin for the Tropospheric Remote Sensing Laboratory
September 2017

FTS Setup

This section covers setting up the spectrometer and preparing for alignment.

Tripod

The tripod for the spectrometer is located in one of the black crates. Set this up so that the marker tape at the top is facing toward the retroreflector location. It is recommended to setup the tripod as low as possible until the pan tilt and spectrometer are mounted on top due to their heavy weight. A mounting plate must be attached to the top of the tripod and these are unique depending on the pan tilt to be used. They are both secured to the tripod in the same way, by separating into two parts and hand tightening the bottom half as shown in Figure 1. The automatic pan tilt mounting plate can be seen attached to the tripod in Figure 2.

Figure 1

Manual Pan Tilt

Place the manual pan tilt head on top of the tripod mounting plate as shown in Figure 3. Use a 5mm hex key to secure it as shown.

Figure 2

Figure 3

Automated Pan Tilt

Place the automated pan tilt head on the tripod and use the tape marker to line up the securing holes as shown in Figure 4. Secure with the eight 8x35mm bolts with an 8mm hex hey. To correctly secure, first place a regular washer, then a locking washer, and finally the bolt.

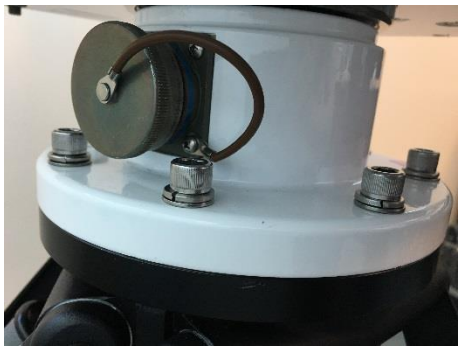

Figure 4

Spectrometer

The spectrometer is located in the other black crate. An extra plate must be added to the bottom of the spectrometer if the automated pan tilt is used and is shown attached in Figure 5. Six 5x15mm bolts are put in with a 5mm hex key into the sliding nuts that are on the bottom of the spectrometer frame. These should be put to their outer most positions then line up the holes on one side of the plate and loosely secure this side with three of the bolts. After that side is secure, but not so tight as to not allowing sliding, move the plate over so that the remaining three holes line up with the other sliding nuts. Screw the remaining three bolts into the holes and then center the plate before finally tightening all six bolts.

Figure 5

Lift the spectrometer onto the top of the pan tilt. The securing method is different depending on the pan tilt used as follows.

Manual Pan Tilt

First ensure the sliding nuts in the bottom of the spectrometer frame are moved all the way to the outside on both sides. Place the spectrometer on top of the pan tilt head and then use six 5x15mm bolts to secure it. To do this, line up the first three holes on one side with the sliding nuts. Place three bolts though the holes in the pan tilt up from the bottom into the spectrometer frame. Loosely tighten these three nuts, then slide the spectrometer over so that the other three holes on the other side line up with the remaining three sliding nuts. Loosely screw three screws into these holes, then center the spectrometer on the pan tilt head by sliding it then tighten all six bolts.

Automated Pan Tilt

Set the spectrometer on top of the pan tilt head. Use the blue marker tape to line up the holes in the plate on the bottom of the spectrometer with the holes in the top of the pan tilt head. Screw the nine 5x50mm bolts from the bottom up into the spectrometer plate with a 5mm hex key as shown in Figure 6.

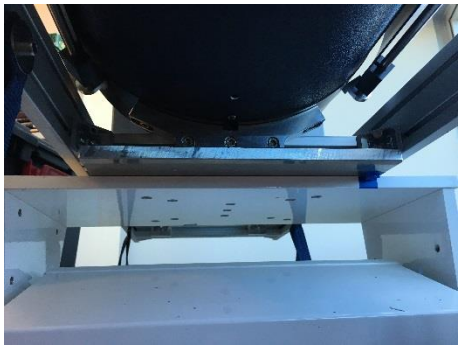

Figure 6

Power Supply

Either a wall adapter mounted on the back end of the spectrometer (left) or a cord from the power supply (right) powers the spectrometer. Both are pictured in Figure 7. The cable required to connect the battery is bright yellow and each lead on it is labeled appropriately. The power supplies must be charged regularly. Each supplies approximately 11 hours of operational time when using the automatic pan tilt and one retroreflector target (no movement of pan tilt during measurement).

Figure 7

A manual for the power supply can be found in the OPS Documentation section of our cloud storage.

Laptop

Connect the Ethernet cable between the spectrometer and the laptop. If using the automatic pan tilt, connect the USB cable from the large yellow cable. All cables are labeled on the ends.

Software called OPUS_RS is used to communicate with the FTS and is used for alignment, data acquisition, and basic retrievals.

Connect the MSR pressure and temperature sensor to the laptop and ensure the sensor leads are in a location that will property represent the path conditions. A manual for the P, T sensor can be found in the OPS documentation section of our cloud storage.

Retroreflector Setup

This section discusses setting up a retroreflector.

Tripod

Place the tripod so that the hole on the upright portion shown in Figure 8 is facing toward the spectrometers location. The hand wheel can raise and lower the tripod by up to 0.5m.

Figure 8

Mounting

The extruding shaft at the bottom of the retroreflector fits into the hole at the top of the tripod. Once in place, line up the hole shown in Figure 8 with the hex screw on the retroreflector. Tighten the hex screw fully with the red handled hex tool located on the bottom brace of the tripod.

Aligning

The retroreflector array should be roughly perpendicular to the line of sight from the spectrometer. To open the retroreflectors protective box, loosen the six screws around the door and slide the metal clasps away from the cover.

Alignment

After the spectrometer and retroreflector are setup, they must be aligned.

Pan Tilt Control

Open OPUS_RS and navigate to the menu 'Options → Pan/Tilt Control' to open the dialog box shown in Figure 9 to control the automatic Pan Tilt. Enter coordinates or click the arrows to move small increments at a time. Clicking and holding in the target circle will allow movement in any direction and the speed increases the further the mouse is from the center of the circle. If using the manual Pan Tilt, simply use the handles to manually adjust tilt and rotation.

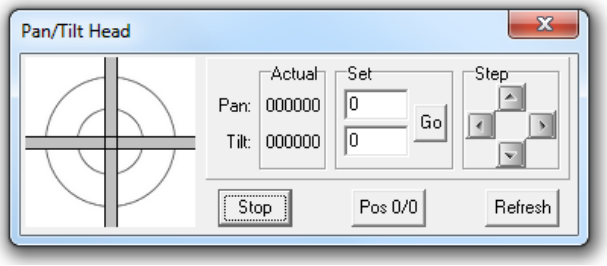

Figure 9

Rough Alignment with Camera

Connect the micro USB cable between the camera, shown in Figure 10, and the laptop. Also, slide the small extruding piece, located on the opposite side of the telescope with respect to the camera, out to allow the camera to view out of the telescope.

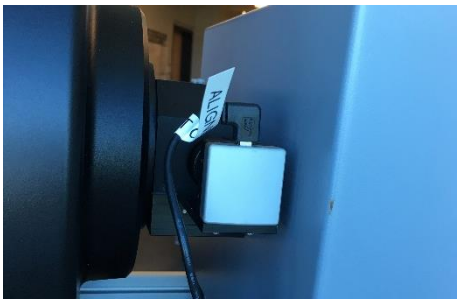

Figure 10

You may need to adjust the exposure and focus of the camera by turning the rings on the camera. Additionally, adjusting the secondary mirror at the front of the spectrometer all the way out improves camera focus. Details on adjusting this mirror are included on the next page.

Open the camera VRmagic CamLab program on the laptop, select the device then press 'Grab'. Press '1' to resize the image so it is visible on the screen as in Figure 11.

Now use either the Pan Tilt dialog box from above or the manual handles on the pan tilt to aim the spectrometer so that the retroreflector is visible at the middle of the image. Ideally, it will be hidden by the black circle in the middle, created by the secondary mirror.

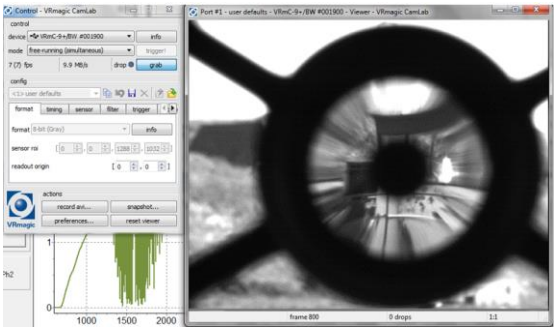

Figure 11

Fine Alignment with Intensity Reading

Ensure sun visor, rain cover, and any other aspects that may affect alignment are in place before beginning fine alignment as they can all cause a major loss of IR signal if moved later.

Now, select the Adjust option in the top right of the OPUS_RS window and a large print number will appear on the screen. This value is an arbitrary IR level and will help fine tune the alignment for optimal signal strength. First, adjust the pan and tilt of the spectrometer using the same method as described above to maximize the number shown on screen.

Figure 12

Figure 13

Use a 2mm hex tool to loosen the set screw on the secondary mirror as shown in Figure 12. Use the red rings on the extruding shaft as a guide when adjusting the mirror. Fewer rings showing will correspond to a shorter path length and more rings showing will maximize the signal for a long path length. Rotate the translation screw, shown in Figure 13 to maximize the IR signal.

Iteratively adjust pan and tilt of the spectrometer and the translation screw on the secondary mirror at least twice to achieve the best alignment.

The value will vary greatly depending on path length and humidity conditions. A typical value of above 10 is acceptable but can vary greatly.

Data Acquisition

Now that the hardware is setup, the software is used to record spectra. Click 'Connect' in the top right of the OPUS_RS window to connect to the spectrometer.

Options Setup

Access the options through the 'Options → Options' menu. An example options dialog box, shown in Figure 15. Set the 'Number of Scans: Sample' number to the number of co-adds you wish to use. Each co-add requires approximately one quarter of a second, so 240 co-adds will average one spectra every minute.

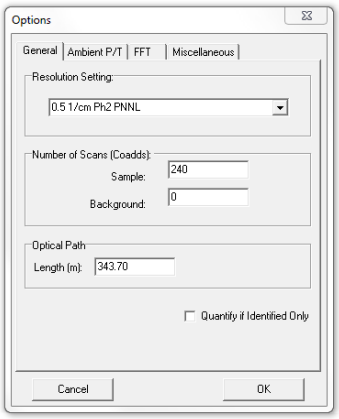

Figure 14

The 'Optical Path' should be set to the total distance between the front of the spectrometer and the face of the retroreflector times two plus 3.7m (to account for path within the telescope). A digital range finder in the lab can be used to find this distance.

Program Mode

In the 'Options → Program Mode Editor' dialog box, a program can be setup to take a measurement using time or number of co-add samples, wait a defined amount of time, or align the spectrometer to a second retroreflector (if using automatic pan tilt). These three options can be done in any order or combination. This dialog box with an example is shown in Figure 16. To turn on the program mode, ensure 'Options → Program Mode Active' is checked off in the menu and if you would like the program to loop, ensure 'Options → Repeat' is checked off as well.

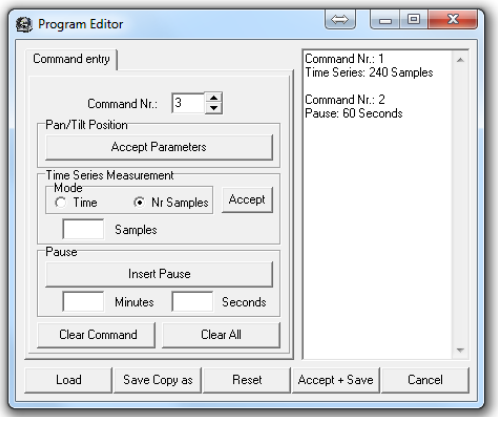

Figure 15

Recording Data

To begin recording data, click the 'START' button in the top right corner of the main OPUS_RS window. Set the desired destination for the data by creating a new folder in the format 'yyyy_mm_dd_Name'. Click 'Okay' to begin measurement. There should be a 'Measurement x of x' in the bottom left of the window if the program is recording spectra.

Periodic Maintenance

Desiccant Drying

There is a capsule of molecular sieve pellets in the spectrometer body to protect the parts inside from excess moisture. This capsule should be changed once the indicator pad has turned blue on all segments. Twist the capsule to remove it from the spectrometer. An oven, as in Figure 17, is used to dry out this desiccant for reuse. This is located in a lab cabinet or if not in the lab available through the Chemistry department (connie.clarke@smu.ca). Empty the capsule, seen in Figure 18, into a lab grade glass dish and place it in the oven as seen in Figure 19. Set the oven at '6' to achieve the appropriate temperature below 150^{o}C and bake it for 24-48 hours. Once they have cooled, pour them back into the capsule and they are ready for reuse.

Figure 16

Figure 17

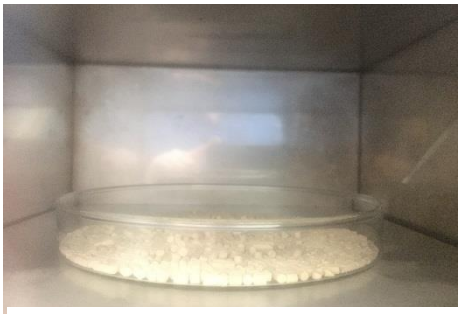

Figure 18

Detector Reconditioning

Detectors require reconditioning that is performed by Bruker after 10000hrs of operation. An approximate time of operation can be found in the 'Report.htm' file from the most recent measurement.

Field Work Supply List

- ☐ Spectrometer Crate
- ☐ Tripod and Pan Tilt Crate
- ☐ Retroreflector and Tripod
- ☐ Loading Ramps
- ☐ Ratchet Straps
- ☐ Power, Data, and Charging Cables
- ☐ P, T Sensor
- ☐ Laptop
- ☐ Power Supply
- ☐ Logbook
- ☐ Assembly Tool Bag

Setup Checklist

- ☐ Secure retroreflector on tripod
- ☐ Setup spectrometer tripod (red tape facing retroreflector)
- ☐ Secure pan-tilt head on tripod (align red tape)
- ☐ Place spectrometer on top of pan-tilt and secure
- ☐ Connect power and data ports
- ☐ Connect to spectrometer to laptop using OPUS_RS (have mini-retro in place)
- ☐ Align spectrometer to retroreflector using camera (2nd mirror out to focus)
- ☐ Move mini-retro out of path
- ☐ Align spectrometer using adjust to maximize the IR signal
- ☐ Iteratively adjust the secondary mirror and pan-tilt to maximize signal
- ☐ Set path length in options menu (2×distance+3.7m)
- ☐ Load 24hr program from desktop
- ☐ Set program mode active and program repeat
- ☐ Start measurement in new folder using format ‘yyyy_mm_dd_name’

Appendix B: HYSPLIT Trajectories

Seven Mile Lake Trajectories

Likelihood of biomass burning emissions arrival defined as:

Weak: > 3 points within 24 km

Moderate: > 3points within 12 km

Strong: >6 points within 12 km

500 m Start Height			100 m Start Height		
Arrival Date [August]	**Arrival Time [hr]**	**Strength**	**Arrival Date [August]**	**Arrival Time [hr]**	**Strength**
10	13	Weak	10	12	Weak
10	15	Weak	10	14	Weak
11	17	Strong	10	15	Weak
11	21	Strong	11	17	Strong
11	20	Strong	11	21	Strong
11	23	Moderate	11	20	Strong
12	1	Weak	11	23	Moderate
12	4	Moderate	12	1	Weak
12	9	Strong	12	5	Moderate
12	11	Strong	12	9	Weak
12	14	Strong	12	11	Weak
12	17	Strong	12	14	Strong
12	18	Strong	12	17	Strong
12	22	Strong	12	18	Strong
13	0	Moderate	12	22	Strong
13	1	Weak	13	0	Moderate
14	20	Strong	14	20	Weak
14	23	Strong	14	23	Strong
15	1	Strong			

The start height does not have a significant effect on modeled arrival times, adding an hour earlier transport on August 10, and 2 hours less on August 14. The result is similar predicted temporal regions for potential detection of biomass burning emissions.

Appendix C: Observatory RFP

The following RFP Scope and Minimum Mandatory Specifications were written with extensive input from the MSc Candidate.

PART 4 – RFP PARTICULARS

4.1 Deliverables

The RFP is an invitation to submit offers for the provision of a modified shipping container to serve as an atmospheric Observatory located on the rooftop of the Student Centre Building at Saint Mary's University.

4.2 Scope

4.2.1 Since its founding in 1802 the University has developed into a mid-sized urban university located in the heart of Halifax and is the second largest educational institution in the province. Over 7,100 full and part time students are enrolled during the academic year and summer sessions, attending day and evening classes on the 39-acre campus in south end of Halifax and more than 900 faculty & staff support programs and operations.

4.2.2 The Observatory will be operated by the research group of the Department of Environmental Science / Department of Astronomy & Physics. The Observatory will initially house an open-path Fourier Transform Infrared (OP-FTIR) spectrometer for continuous atmospheric trace gas measurements in the atmospheric path between the Observatory and a retroreflector mounted on a nearby building. Infrared radiation is strongly attenuated by general purpose window materials and for this reason the windows must open as described in section 4.3.12 for measurements using the Open-path Fourier Transform Infrared. The Observatory will also be used, directly and/or indirectly, as a teaching facility for University students.

4.2.3 The University will be responsible for all roofing modifications required to place the Observatory on the Student Centre roof, as well as for connecting power, fire suppression, and internet to the Observatory through provisioning manufactured by the Contractor. After contract award, further communication between the Contractor and the University is expected to coordinate Observatory manufacturing and placement on the roof by the Contractor and roof modifications.

4.2.4 The Observatory will be installed on the rooftop of the Student Centre Building. It will be installed inside a wooden curb provided by the University. The Contractor is responsible for providing anchoring for the Observatory to anchor the wooden curb. The Student Centre Building is located at Saint Mary's University, ,5916 Inglis Street, Halifax, Nova Scotia, Canada. See Appendix B (Delivery Requirements) for diagrams and dimensions of the receiving location.

4.2.5 The Contractor will be required to store the Observatory at their location until the roofing modification work is completed and the University is prepared for arrival and placement of the Observatory on top of the Student Centre building.

4.2.6 The Contractor is responsible for providing the proper manpower and equipment to off-load and place the Observatory on top of the Student Centre Building

4.2.7 It is the Contractor's responsibility to arrange full and complete protection of all shipments to the University and to make all necessary arrangements to offload and place the equipment in the required location. No additional charges of any kind, including charges relating to boxing, packaging or cartage will be allowed unless specifically agreed to in writing by the University.

4.2.8 Unless otherwise specified, all shipments shall be DAP (delivered at place) offloaded and placed on the roof of the Student Centre Building.

4.2.9 The Contractor is required to familiarize themselves with the layout features and characteristics of the campus which could affect delivery.

4.2.10 The Contractor is responsible to remove and dispose of any crating, wrapping and packaging off campus in a responsible manner.

4.2.11 The University reserves the right to reject in part or in whole, goods received in a damaged condition. All claims for damage or loss in transit must be initiated by the Contractor.

4.2.12 Regardless of payment, all goods and/or services shall be subject to inspection and approval by the University without limitation as to time. The University may reject the goods and/or services, in whole or in part, and/or terminate an order if, in the opinion of the University, the goods and/or services, in whole or in part, are unsatisfactory, non-conforming to the order specifications, or if the Contractor has breached any term or condition of an order.

4.2.13 In the case of rejected goods, the University may either return the goods to the Contractor at their risk and expense, or, advise the Contractor to remove the rejected goods, at their risk and expense, whereupon any responsibility of the University with respect to the rejected goods shall absolutely cease.

4.2.14 Delivery will be considered complete and ownership pass to the University when the equipment is assembled, installed, fully functional, orientation is completed and a successful manufacturer's test is performed, as determined by the Department of Environmental Science designate (Prof. Wiacek), and Facilities Management engineers and architects. Acceptance by the University will include testing of compliance with applicable CSA standards and manufacturer's performance specifications. Any findings, not in compliance with specifications or applicable standards, will be the responsibility of the Contractor to rectify these deficiencies.

4.2.15 On-site, intro-level (first-user) orientation is required to be provided by the Contractor to operate the equipment, within a reasonable time after delivery.

4.2.16 An Operators Manual should be included for all relevant subsystems of the Observatory, especially the HVAC system. Failure to include required documentation may delay final approval and payment.

4.2.17 The Contractor will be required to arrange after sale warranty service for the equipment ordered and installed for a minimum period of one (1) year as a result of this RFP.

4.2.18 The warranty period shall begin on the date the equipment has successfully passed the acceptance tests.

4.2.19 As final prices are unknown at this time, the University reserves the right to modify the equipment specification or to remove items from the equipment list in order to correspond with available funding. Proponents must indicate if their proposal prices will change in the event that components are removed from the equipment list, if applicable.

4.3 Minimum Mandatory Specification:

The specifications listed are to establish acceptable quality and performance standards. Alternatives will be considered provided they meet or exceed these standards and are advantageous to the University in terms of cost or other relevant factors. All proposed equivalents must be identified and are subject to University approval.

.1 The Observatory will be based on a new or like new single-journey steel shipping container. Proponent to verify single journey (if applicable).

.2 All installed components and subsystems must be new.

.3 Modifications to the container must follow the general intent of the DNV 2.7-1 Offshore Container standard and allow the structure to be transported to the University by a flatbed truck and be lifted by a crane onto the rooftop of a 5-story building.

.4 Contractor workshop must be Canadian Welding Bureau certified. Certification document should be provided with RFP submission.

.5 Contractor must supply engineering drawings of container-based Observatory to the University for approval prior to fabrication (ISO9001:2008 Certified Quality System).

.6 Observatory exterior dimensions must be 24' long (for structural reasons), 8' wide, and 8'6" high.

.7 Observatory will be insulated for occupied space (R24) with compact materials.

.8 Interior walls and floor will be finished with, at a minimum, water-resistant materials, covering all structural components and insulation.

.9 Floor drain(s) will be installed to prevent accumulation of water on floor in case of water ingress during measurements using the OP-FTIR Spectrometer in rainy weather.

.10 A thermally insulated metal door with a minimum width of 32" and height of 80" will be located on a long wall of the Observatory. See provisional design Appendix C.

.11 Door will be supplied with lever handle and a BEST cylinder lock, with a BEST cylinder ready to accept a University-supplied core.

.12 The Observatory will have 6 windows of awning type that open outward to a minimum of 90° upward from the closed position and remain in the open position during reasonable (e.g., < 50 km/h) wind speeds (Appendix C). The windows will be at least 4' wide by 2' tall and installed at a vertical height that is approved by the University. Windows are to be thermally efficient to a degree that is practical under all design constraints. One window will be centered on each short end of the Observatory, three will be evenly disturbed across the wall opposite the door location, and one window will share the wall with the door. Exact window dimensions meeting the minimum requirements and their placement will be agreed upon after award of contract. Retaining clips to be installed on the interior of windows to allow a ¼" thick modified window covering (supplied by the University) to fit securely in or against the window frame. The purpose of the modified window covering is to limit the open window area to only the much smaller area required to pass a 12" diameter infrared radiation beam into the open atmosphere.

.13 All electrical devices, appliances, cables and equipment must be certified to Canadian Standards, bearing one of the marks or labels that are approved by the Provincial Chief Electrical Inspector for use in Nova Scotia. http://novascotia.ca/lae/electricalsafety/esb0304.asp.

.14 The Observatory will be equipped with a 120/208v, 3ph, 4W, 100A panelboard, equivalent to Eaton Cat. No. P1aL4A1-42 c/w 100A HJD Main breaker & TVSS protection.

.15 The Observatory will be equipped with an HVAC system with a working range between -23°C to 46°C with the ability to maintain the interior of the laboratory at 24°C during summer months and 21°C during winter months. The HVAC system should be designed to all windows closed in the Observatory. The manufacturer of the HVAC system must be Daikin, Mitsubishi Electric, Trane, ClimateMaster or equivalent. The HVAC system shall also be installed, tested and commissioned in compliance with the manufacturer's recommendations. The Contractor shall provide a complete installation and operation manual for the equipment upon delivery of equipment and shall ensure the equipment is installed such that all service clearances (both required and recommended by the manufacturer) are met. Equipment shall be constructed to the requirements of Air-Conditioning, Heating, and Refrigeration Institute (AHRI), Canadian Standards Association (CSA) and Underwriters Laboratories of Canada (ULc). The unit is to be complete with a spare set of dry contacts for monitoring by the University Building Automation System (BAS).

.16 Lighting will be installed so that a maintained minimum average illuminance level of 50Fc is achieved. This shall be accomplished using EEL Model No. VT40LED04(P) or equivalent. Fixtures are to be controlled via a switch with dimming capability and occupancy sensor.

.17 Six (6) 15A, 120V wall outlets will be distributed around Observatory interior with ground fault protection.

.18 One (1) 15A, 120V wall outlet with metal extra-duty while in-use cover and ground fault protection (complying with rule 26-702(2) of the CEC) will be located on the long exterior Observatory wall that also includes the door.

.19 One (1) 15A, 240V wall outlet will be located in Observatory interior, with ground fault protection.

.20 A minimum of four data outlets will be installed in the Observatory interior allowing connection to building LAN via a conduit sleeve. Installation and termination of CAT6 by the University.

.21 The Contractor will communicate with the University to a reasonable extent regarding provisioning indicated in the supplied drawings (see 4.3.5 above) for connection of building power, fire suppression, sprinklers and data ports to Observatory.

.22 Emergency lighting will be installed in Observatory interior.

.23 A 24" x 24" rooftop hatch will be installed in a manner making it waterproof and non-pooling of rain or melt water. It will be able to accommodate the addition of a future dome permitting zenith sky observations. See provisional design Appendix C

.24 Lockable folding ladder steps for accessing the roof will be installed on the long Observatory wall with the door (Appendix C), similar to the design in Figure 1 of Geibel et al., 2010 (https://www.atmos-meas-tech.net/3/1363/2010/amt-3-1363-2010.pdf).

.25 A rooftop anchoring system that meets applicable standards will be installed.

.26 Two rooftop goose necks of approximately Ø10" will be installed on the Observatory, with the ability to shut the openings.

.27 Emergency and electrical name plating to clearly label exits, electrical outlets, and electrical panels and data ports in the Observatory.

.28 Exterior of Observatory will be fully painted with marine grade paint, applied according to paint manufacturer's recommendations, in a colour approved by the University.

.29 Mounting location for a 10' tall (height above Observatory roof) Ø2" wind mast (provided by the University at a later date) using three collars or a similar solution and sharing the long Observatory wall with the door.

Appendix D: Retroreflector Door Force Requirements

The following calculation determines the approximate force required by the linear actuators to open the retroreflector door.

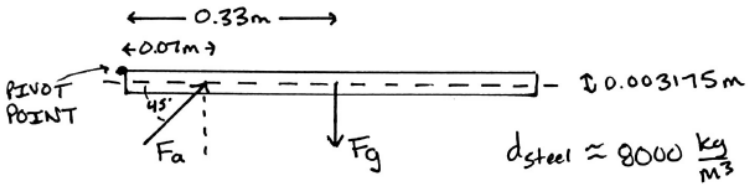

$$F_g = mg$$
$$= dVg$$
$$= 8000\ ^{kg}/_{m^3} \cdot 0.66m \cdot 0.66m \cdot 0.003175m \cdot 9.81\ ^{m}/_{s^2}$$
$$= 109\ N$$

$$\tau_a = \tau_g$$
$$F_a \sin 45^\circ d_a = F_g d_g$$
$$F_a = \frac{F_g\, d_g}{\sin 45^\circ\, d_a}$$
$$= \frac{109N \cdot 0.33m}{\sin 45^\circ \cdot 0.07m}$$
$$= 724\ N$$

$$F_a = 724N \cdot \frac{1lbf}{4.45\ N} = 162\ lbf$$

Two actuators used $\therefore > 81$ lbf each

Installed actuators with max load 270 lbf.
(~3x force needed)

Appendix E: Observatory Automation Solution Parts List

Part	Description	Vendor
Linear Actuators	Applies the force necessary to lift retroreflector enclosure door. · 270lb maximum force · 4” stoke · 12V <3A	Princess Auto Part No 8507816
Linear Actuator Brackets	Attach the linear actuators to the door and retroreflector enclosure frame.	firgelliauto.ca Part No MB1
Battery	Supplies the retroreflector enclosure with power for mobile use. · 12V · 7.2Ah	Digikey.ca Part No P078-ND
Power Supply	Supplies the retroreflector enclosure with power when a building source is available. · 120VAC input · 12VDC output · 8A	Digikey.ca Part No 1866-2044-ND
RF Control System	Provides wireless control between the observatory and the retroreflector. · 12V	RFcontrolsystem.com Part No 0020480 (S2PF-DC12/24)
Numato USB Relay Module	Interfaces the laptop to the RF transmitter. · 8 relay outputs	Numato.com Part No RL80001
Power Supply for Transmitter	Supplies Relay Board and Transmitter · 12V · 100W · AC/DC Converter	Digikey.ca Part No 1145-1070-ND

Appendix F: Weather Control Python Script

```
import sys, serial, urllib.request, threading, time, itertools, json
from tkinter import *
from tkinter import ttk
from time import sleep

import datetime

class control(object):
# (up = gpio 5) (down = gpio 6) (stop = gpio 7)
    def up(*args):
        try:
            serPort = serial.Serial('COM10', 19200, timeout=1)

            serPort.write("gpio clear 5\r".encode())
            serPort.write("gpio clear 6\r".encode())
            serPort.write("gpio clear 7\r".encode())

            serPort.write("gpio set 7\r".encode())
            sleep(0.5)
            serPort.write("gpio clear 7\r".encode())
            sleep(0.5)

            serPort.write("gpio set 5\r".encode())
            sleep(0.5)
            serPort.write("gpio clear 5\r".encode())
            sleep(30)

            serPort.write("gpio set 7\r".encode())
            sleep(0.5)
            serPort.write("gpio clear 7\r".encode())

            serPort.close()
        except:
            messagebox.showinfo("Error", "Can't connect to RF transmitter.")
            pass

    def down(*args):
        try:
            serPort = serial.Serial('COM10', 19200, timeout=1)

            serPort.write("gpio clear 5\r".encode())
            serPort.write("gpio clear 6\r".encode())
            serPort.write("gpio clear 7\r".encode())

            serPort.write("gpio set 7\r".encode())
            sleep(0.5)
            serPort.write("gpio clear 7\r".encode())
            sleep(0.5)

            serPort.write("gpio set 6\r".encode())
            sleep(0.5)
            serPort.write("gpio clear 6\r".encode())
            sleep(30)

            serPort.write("gpio set 7\r".encode())
            sleep(0.5)
            serPort.write("gpio clear 7\r".encode())

            serPort.close()
```

```
        except:
            messagebox.showinfo("Error", "Can't connect to RF transmitter.")
            pass

    def stop(*args):
        try:
            serPort = serial.Serial('COM10', 19200, timeout=1)

            serPort.write("gpio clear 5\r".encode())
            serPort.write("gpio clear 6\r".encode())
            serPort.write("gpio clear 7\r".encode())

            serPort.write("gpio set 7\r".encode())
            sleep(0.5)
            serPort.write("gpio clear 7\r".encode())

            serPort.close()
        except:
            messagebox.showinfo("Error", "Can't connect to RF transmitter.")
            pass

class refresh(object):

    def update(*args):
        while True:
            try:
                BGO_url = 'http://www.ap.smu.ca/~bgo/cloud/boltwood.txt'
                with urllib.request.urlopen(BGO_url) as url:
                    BGO_data = url.read().decode('utf-8')
                    BGO_data = BGO_data[0:len(BGO_data)-2].split(',')
                    BGO_condition = BGO_data[2].title()
            except:
                BGO_condition = 'Unavailable'

            BGO_text     =     ttk.Label(mainframe,     text='BGO     Conditions:
').grid(column=1, row=1, sticky=W, padx=(0,25))
            BGO_state = ttk.Label(mainframe, text=BGO_condition).grid(column=2,
row=1, sticky=W, padx=(0,25))

            try:
                WU_url                                                          =
'http://api.wunderground.com/api/b786d506854ea6da/geolookup/conditions/q/pws:INO
VASCO115.json'
                with urllib.request.urlopen(WU_url) as url:
                    WU_data = url.read().decode('utf8')
                    WU_data = json.loads(WU_data)
                    WU_condition = WU_data['current_observation']['weather']
                    WU_time                                                     =
WU_data['current_observation']['observation_time_rfc822']
                    WU_temp = WU_data['current_observation']['temp_c']
                    WU_pressure = WU_data['current_observation']['pressure_mb']
                    WU_humidity                                                 =
WU_data['current_observation']['relative_humidity']
                    WU_percip                                                   =
WU_data['current_observation']['precip_1hr_metric']
                    WU_wind = WU_data['current_observation']['wind_gust_kph']
            except:
                WU_condition = 'Unavailable'
                WU_time = 'Unavailable'
                WU_temp = 'Unavailable'
                WU_pressure = 'Unavailable'
                WU_humidity = 'Unavailable'
                WU_percip = 'Unavailable'
```

```
                WU_wind = 'Unavailable'

            ttk.Label(mainframe, text='WU Conditions: ').grid(column=1, row=2,
sticky=W, padx=(0,25))
            ttk.Label(mainframe,    text=WU_condition).grid(column=2,    row=2,
sticky=W, padx=(0,25))

            if ('Clear' in BGO_condition) or ('Cloudy' in BGO_condition) or
('Verycloudy' in BGO_condition):
                ttk.Label(mainframe,  text='Status:  ').grid(column=1,  row=3,
sticky=W, padx=(0,25))
                ttk.Label(mainframe, text='Good       ').grid(column=2, row=3,
sticky=W, padx=(0,25))
                ttk.Label(mainframe,  text='Retro:  ').grid(column=1,  row=4,
sticky=W, padx=(0,25))
                ttk.Label(mainframe, text='Open       ').grid(column=2, row=4,
sticky=W, padx=(0,25))
                control.up()
            elif ('Wet' in BGO_condition) or (float(WU_wind) > 50) or
(float(WU_percip) > 0.5) or ('Snow' in WU_condition) or ('Ice' in WU_condition)
or ('Freezing' in WU_condition) or ('Hail' in WU_condition):
                ttk.Label(mainframe,  text='Status:  ').grid(column=1,  row=3,
sticky=W, padx=(0,25))
                ttk.Label(mainframe, text='Bad        ').grid(column=2, row=3,
sticky=W, padx=(0,25))
                ttk.Label(mainframe,  text='Retro:  ').grid(column=1,  row=4,
sticky=W, padx=(0,25))
                ttk.Label(mainframe, text='Closed     ').grid(column=2, row=4,
sticky=W, padx=(0,25))
                control.down()
            else:
                ttk.Label(mainframe,  text='Status:  ').grid(column=1,  row=3,
sticky=W, padx=(0,25))
                ttk.Label(mainframe, text='Unknown      ').grid(column=2, row=3,
sticky=W, padx=(0,25))
                ttk.Label(mainframe,  text='Retro:  ').grid(column=1,  row=4,
sticky=W, padx=(0,25))
                ttk.Label(mainframe, text='Closed     ').grid(column=2, row=4,
sticky=W, padx=(0,25))
                control.down()

            ttk.Label(mainframe,    text='BGO    Data').grid(column=1,    row=5,
pady=(25,0))
            ttk.Label(mainframe,    text='WU    Data').grid(column=2,    row=5,
pady=(25,0), columnspan=2)
            ttk.Label(mainframe,                                    text=BGO_data[0]+'
'+BGO_data[1]).grid(column=1, row=6)
            ttk.Label(mainframe,       text=WU_time).grid(column=2,       row=6,
columnspan=2)

            date_time=datetime.datetime.now().strftime("%I:%M%p on %B %d, %Y")

            with open('weatherlog.txt', 'a+') as f:
                f.write(str(date_time) + '\tBGO: ' + str(BGO_data[0]) + ' ' +
str(BGO_data[1]) + ' ' + str(BGO_condition) + '\t\tWU: ' + str(WU_time) + ' ' +
str(WU_condition) + ' ' + str(WU_wind) + 'km/h ' + str(WU_percip) + 'mm\n')

            sleep(299)

if __name__=='__main__':

    threadObj = threading.Thread(target=refresh.update)
    threadObj.start()
```

```
    root = Tk()
    root.wm_title("Retroreflector Control")

    mainframe = ttk.Frame(root, padding="25 25 25 25")
    mainframe.grid(column=0, row=0, sticky=(N, W, E, S))
    mainframe.columnconfigure(0, weight=1)
    mainframe.rowconfigure(0, weight=1)

    up_btn = ttk.Button(mainframe, text="Up", command=control.up).grid(column=3,
row=1)
    down_btn           =           ttk.Button(mainframe,           text="Down",
command=control.down).grid(column=3, row=2)
    stop_btn           =           ttk.Button(mainframe,           text="Stop",
command=control.stop).grid(column=3, row=3)

    for child in mainframe.winfo_children(): child.grid_configure(padx=5, pady=5)
    root.bind('<Return>', control.stop)
    root.mainloop()
```

5. References

Baldauf, R., Thoma, E., Khlystov, A., Isakov, V., Bowker, G., Long, T., & Snow, R. (2008). Impacts of noise barriers on near-road air quality. Atmospheric Environment, 42(32), 7502-7507.

Banwell, C. N., & MacCash, E. M. (1994). Fundamentals of Molecular Spectroscopy (4 ed.). London: McGraw-Hill.

Bradley, K. S., Brooks, K. B., Hubbard, L. K., Popp, P. J., & Stedman, D. H. (2000). Motor vehicle fleet emissions by OP-FTIR. Environmental Science & Technology, 34(5), 897-899.

Bruker. (2013). OPS flyer.

Bruker. (2015). OPS manual.

CERC.OCEAN's Container Lab is Headed to St. John's. (2017, April 19). Dalhousie University News. Retrieved from https://www.dal.ca/diff/cerc/news/2017/04/19/cerc_ocean_s_container_lab_is_headed_to_st__john_s.html

IPCC. (2013) Summary for Policymakers. In: Climate Change 2013: The Physical Science Basis. Contribution of Working Group I to the Fifth Assessment Report of the Intergovernmental Panel on Climate Change [Stocker, T.F., D. Qin, G.-K. Plattner, M. Tignor, S.K. Allen, J. Boschung, A. Nauels, Y. Xia, V. Bex and P.M. Midgley

(eds.)]. Cambridge University Press, Cambridge, United Kingdom and New York, NY, USA.

Denise Lineberry. (2016, May 19). Canadian fire plume detected during NAAMES transit flight. NASA Blog. Retrieved from https://blogs.nasa.gov/earthexpeditions/2016/05/19/canadian-fire-plume-detected-during-naames-transit-flight/

Flesch, T. K., Baron, V. S., Wilson, J. D., Griffith, D. W. T., Basarab, J. A., & Carlson, P. J. (2016). Agricultural gas emissions during the spring thaw: Applying a new measurement technique. Agricultural and Forest Meteorology, 221, 111-121.

Flesch, T. K., Basarab, J. A., Baron, V. S., Wilson, J. D., Hu, N., Tomkins, N. W., & Ohama, A. J. (2017). Methane emissions from cattle grazing under diverse conditions: An examination of field configurations appropriate for line-averaging sensors. Agricultural and Forest Meteorology.

Franklin, J. E., Drummond, J. R., Griffin, D., Pierce, J. R., Waugh, D. L., Palmer, P. I., . . . Saha, A. (2014). A case study of aerosol scavenging in a biomass burning plume over eastern Canada during the 2011 BORTAS field experiment. Atmospheric Chemistry and Physics, 14(16), 8449-8460.

Geibel, M. C., Gerbig, C., & Feist, D. G. (2010). A new fully automated FTIR system for total column measurements of greenhouse gases. Atmospheric Measurement Techniques, 3(5), 1363-1375.

Griffith, D. (1996). Synthetic calibration and quantitative analysis of gas-phase FT-IR spectra. Applied Spectroscopy, 50(1), 59-70.

Griffith, D. (2012). Computational retrieval of trace gas concentrations from FTIR spectra [draft].

Griffith, D. (2016). MALT55 User Guide.

Griffiths, P. (2007). In De Haseth J. A. (Ed.), Fourier transform infrared spectrometry (2nd ed.). Hoboken, N.J.: Hoboken, N.J. Wiley-Interscience.

Griffiths, P., Shao, L., & Leytem, A. (2009). Completely automated open-path FT-IR spectrometry. Analytical and Bioanalytical Chemistry, 393(1), 45-50.

Halifax, Metro. (2016, August 10). Smoke drifts into Halifax as wildfires continue to grow across Nova Scotia. Metro Halifax. Retrieved from http://www.metronews.ca/news/halifax/2016/08/10/smoke-drifts-into-halifax-wildfires-to-grow-in-nova-scotia.html

Jackson, J. M., Liu, H., Laszlo, I., Kondragunta, S., Remer, L. A., Huang, J., & Huang, H. (2013). Suomi-NPP VIIRS aerosol algorithms and data products. Journal of Geophysical Research: Atmospheres, 118(22), 12,689.

Jacob, D. J. (1999). Introduction to Atmospheric Chemistry. Princeton, N.J.: Princeton, N.J. Princeton University Press.

Jarvis. (2003). Open path spectrophotometry (UV, IR, FT-IR). Instrument engineers' handbook - process measurement and analysis, volume 1 (4th ed., pp. 1). Instrument Engineers Handbook: Taylor & Francis.

Millet, D. B., Goldstein, A. H., Holzinger, R., Williams, B. J., Allan, J. D., Jimenez, J. L., Stohl, A. (2006). Chemical characteristics of North American surface layer outflow: Insights from Chebogue Point, Nova Scotia. Journal of Geophysical Research: Atmospheres, 111(D23).

Nova Scotia Environment. (2016). Air monitoring network map. Retrieved from http://www.novascotia.ca/nse/air/docs/AirMonitoringNetworkMap.pdf

Paton-Walsh, C., Smith, T. E. L., Young, E. L., Griffith, D. W. T., & Guérette, É. (2014). New emission factors for Australian vegetation fires measured using open-path Fourier transform infrared spectroscopy – part 1: Methods and Australian temperate forest fires. Atmospheric Chemistry and Physics, 14(20), 11313-11333.

Purcell, J. (2016). Comparison of first SMU open-path Fourier transform infrared (OP-FTIR) spectrometer measurement results with national air pollution surveillance (NAPS) air quality measurements in Halifax. BSc Thesis: Saint Mary's University.

Remer, L. A., Kaufman, Y. J., Tanré, D., Mattoo, S., Chu, D. A., Martins, J. V., Holben, B. N. (2005). The MODIS aerosol algorithm, products, and validation. Journal of the Atmospheric Sciences, 62(4), 947-973.

Rothman, L. S., Gordon, I. E., Babikov, Y., Barbe, A., Chris Benner, D., Bernath, P. F., Wagner, G. (2013). The HITRAN2012 molecular spectroscopic database. Journal of Quantitative Spectroscopy and Radiative Transfer, 130, 4-50.

Shepardson, D. P. (2001). Assessment in science. Dordrecht: Kluwer.

You, Y., Staebler, R., Moussa, S., Su, Y., Munoz, T., Stroud, C., Moran, M. (2017). Long-path measurements of pollutants and micrometeorology over Highway 401 in Toronto. Atmospheric Chemistry and Physics, 17(22), 14119-14143.